NEUROSCIENCE

Upper cortical layer–driven network impairment in schizophrenia

Mykhailo Y. Batiuk[1]†‡, Teadora Tyler[2]†, Katarina Dragicevic[1], Shenglin Mei[3], Rasmus Rydbirk[1], Viktor Petukhov[1], Ruslan Deviatiiarov[4,5], Dora Sedmak[6], Erzsebet Frank[2], Virginia Feher[2], Nikola Habek[6], Qiwen Hu[3]§, Anna Igolkina[3,7], Lilla Roszik[2], Ulrich Pfisterer[1], Diego Garcia-Gonzalez[1], Zdravko Petanjek[6], Istvan Adorjan[2]*, Peter V. Kharchenko[3]*, Konstantin Khodosevich[1]*||

Schizophrenia is one of the most widespread and complex mental disorders. To characterize the impact of schizophrenia, we performed single-nucleus RNA sequencing (snRNA-seq) of >220,000 neurons from the dorsolateral prefrontal cortex of patients with schizophrenia and matched controls. In addition, >115,000 neurons were analyzed topographically by immunohistochemistry. Compositional analysis of snRNA-seq data revealed a reduction in abundance of GABAergic neurons and a concomitant increase in principal neurons, most pronounced for upper cortical layer subtypes, which was substantiated by histological analysis. Many neuronal subtypes showed extensive transcriptomic changes, the most marked in upper-layer GABAergic neurons, including down-regulation in energy metabolism and up-regulation in neurotransmission. Transcription factor network analysis demonstrated a developmental origin of transcriptomic changes. Last, Visium spatial transcriptomics further corroborated upper-layer neuron vulnerability in schizophrenia. Overall, our results point toward general network impairment within upper cortical layers as a core substrate associated with schizophrenia symptomatology.

INTRODUCTION

Schizophrenia is a severe mental brain disorder, which affects around 20 million people worldwide (*1*). Because of the high complexity of neuronal circuits that underlie cognitive abnormalities in schizophrenia, the etiology of schizophrenia is still poorly understood (*2*, *3*). It has been proposed that schizophrenia may arise because of the susceptibility of the developing brain to adverse genetic and environmental factors that perturb embryonic brain development and postnatal maturation of brain circuits (*2*–*4*). However, the impact of these adverse factors will vary from cell to cell, and some cell types should be more susceptible and have a stronger contribution to schizophrenia (*5*, *6*).

Animal models provided an initial insight into cell types that could be affected by schizophrenia-inducing adverse factors. A number of animal models have been generated so far to mimic genetic and environmental perturbations associated with schizophrenia in humans (*7*–*12*). Several brain cell types were found to contribute to the phenotypic impairments of these model animals, of which cortical γ-aminobutyric acid–expressing (GABAergic) interneurons have received the most attention. In particular, parvalbumin (PV)–expressing interneurons were shown to be morphologically and functionally impaired in both genetic and environmental models of schizophrenia (*7*, *9*–*11*, *13*). Besides function and morphology, their distribution across cortical layers and overall density in the cortex were also found altered (*9*, *10*).

Despite the admittedly crucial role of PV interneurons in schizophrenia pathogenesis, there are more and more indications that other neuronal subtypes might have an equal, if not larger, impact on circuit function in schizophrenia. Another large family of GABAergic interneurons that express somatostatin (SST) has a key role in the circuitry controlling sensory information processing that is impaired in schizophrenia (*14*), and a growing body of evidence suggests the involvement of SST interneurons in schizophrenia-related impairments in animal models (*9*, *15*, *16*). Furthermore, animal model work shows that cortical principal neurons might have a primary role in the alteration of neuronal circuitry in schizophrenia (*8*).

A number of recent studies in postmortem human brain tissue from patients with schizophrenia also support the idea that the complexity of neuronal circuit impairment in schizophrenia goes beyond PV interneurons. The morphology and gene expression of human cortical PV interneurons are changed in schizophrenia (*17*–*19*). However, these changes occur in other subtypes of GABAergic interneurons as well, such as SST interneurons that show signs of impairment in the cortex of patients with schizophrenia (*19*, *20*). Moreover, changes in non-PV interneurons in the brains of patients with schizophrenia extend to other brain regions—the large cholinergic and calretinin (CR)–expressing GABAergic interneurons and small CR GABAergic interneurons showed reduced densities in the striatum (*21*, *22*), and the density of SST-expressing GABAergic interneurons was found to be reduced in the amygdala (*23*) of patients with schizophrenia. Thus, it seems obvious that the changes in schizophrenia circuits are highly complex and involve a number of neuronal subtypes.

While studies in both animal models and human brains provided us with immense knowledge of structural and functional impact of schizophrenia on neuronal circuits, most of these studies were

[1]Biotech Research and Innovation Centre (BRIC), Faculty of Health and Medical Sciences, University of Copenhagen, 2200 Copenhagen, Denmark. [2]Department of Anatomy, Histology and Embryology, Semmelweis University, Budapest H-1085, Hungary. [3]Department of Biomedical Informatics, Harvard Medical School, Boston, MA 02115, USA. [4]The National Center for Personalized Medicine of Endocrine Diseases, Moscow 115478, Russia. [5]Kazan Federal University, Kazan 420043, Russia. [6]Croatian Institute for Brain Research and Center of Excellence for Basic, Clinical and Translational Neuroscience, School of Medicine, University of Zagreb, Zagreb 10000, Croatia. [7]St. Petersburg Polytechnical University, St. Petersburg 195251, Russia.
*Corresponding author. Email: adorjan.istvan@med.semmelweis-univ.hu (I.A.); peter.kharchenko@post.harvard.edu (P.V.K.); konstantin.khodosevich@bric.ku.dk (K.K.)
†These authors contributed equally to this work.
‡Present address: École Polytechnique Fédérale de Lausanne (EPFL), CH-1015 Lausanne, Switzerland.
§Present address: Bristol Myers Squibb, Seattle, WA, USA.
||Lead contact.

focused on one or a few specific neuronal subtypes. A more unbiased approach that analyzes changes in all cells in a brain region affected by schizophrenia will help to identify a complete picture of molecular and cellular changes and further understand the etiology of schizophrenia. Some effort has been made for less biased characterization of schizophrenia-associated changes in brain cells using bulk transcriptomics on postmortem human brain tissue (*24*–*26*). These studies identified a number of genes that are involved in developmental processes, such as cell proliferation, differentiation, migration, and maturation, that changed their expression in the brains of patients with schizophrenia. Nevertheless, while these studies identified important generalized effects of schizophrenia on cortical tissue, they lacked resolution to pinpoint the cell types most affected in schizophrenia and reveal schizophrenia-associated gene expression involved in abnormal neuronal circuitry possibly underlying symptoms.

To reveal in an unbiased way the impact of schizophrenia on the whole diversity of neuronal subtypes in the cortex, we carried out single-nucleus RNA sequencing (snRNA-seq) on postmortem brain tissue from well-characterized patients with schizophrenia and age/sex-matched control cases with no history of mental illness. Using several computational approaches to assess how schizophrenia affects the composition of neuronal subtypes in the cortex, we identify schizophrenia-associated changes across all cortical layers with the highest perturbations for neuronal subtypes in the upper layers. Our analysis reveals a reduction in proportion of neurons across all families of GABAergic neurons and an increase in specific subtypes of principal neurons with the strongest changes in upper layers. We have further substantiated these findings by histological analysis showing density reduction in upper-layer subtypes of GABAergic interneurons. At the transcriptomic level, most changes are related to up-regulation of neurotransmission and developmental processes and down-regulation of metabolism genes, indicating active changes in information processing and transfer through schizophrenia-associated circuits along with impairment in energy production in neurons, a common finding across neuronal subtypes. Last, using spatial transcriptomics, we validate gene expression and neuronal composition changes in circuits affected by schizophrenia.

RESULTS

Neuronal subtypes from the upper cortical layers show the largest compositional and gene expression alterations in schizophrenia

The dorsolateral prefrontal cortex (DLPFC) from Brodmann area 9 (BA9) of patients with schizophrenia and matched controls (9 and 14 individuals, respectively) was analyzed by snRNA-seq throughout this study. BA9 was chosen on the basis of the functional and anatomical data from schizophrenia patients showing abnormal brain activity, neuronal morphology, and gene expression in this area relative to matched control brains (*27*–*29*). Importantly, our sample cohort was formed balancing the potential confounders, including the age of sample donors (the vast majority of samples were from 55- to 70-year-old subjects), their postmortem intervals (PMIs; 1 to 23 hours), and other confounders (tables S1 and S2) (fig. S1, A and B). Moreover, multidimensional scaling plots that visualize samples based on the similarity of their transcriptome showed lack of effects for tissue source, age, first-symptoms age, and duration of disease on transcriptomic distance between control and schizophrenia samples (fig. S1C).

For each sample, microdissected cortical columns containing all layers were sorted for neuronal nuclei based on the expression of the neuronal marker NeuN (Fig. 1A and fig. S2A). $NeuN^+$ sorting strategy was designed such that there is only a minor number of neuronal nuclei in discarded $NeuN^-$ fraction, and >95% of neurons are sorted out in $NeuN^+$ fraction as validated by us before (*30*), and snRNA-seq was performed using 10x Chromium v3 assay. In total, we sequenced 225,012 nuclei (with 54,230 reads per nucleus), of which 209,053 (81,817 from schizophrenia and 127,236 control nuclei) passed quality control analysis and doublet filtering and were of high quality (with ~12,000 median Unique molecular identifiers (UMIs) and ~4400 median genes detected per nucleus; fig. S2, B to E, and table S1).

To annotate the neuronal populations in a consistent manner, different samples were first aligned in a way that minimized the impact of the interindividual variation, and clusters of nuclei were determined uniformly across the entire sample collection (*31*). The clusters were annotated on the basis of known layer-specific genes for principal neurons, subtype-specific genes for GABAergic interneurons from previous studies (*30*, *32*), as well as cluster-specific markers (table S3; see also correspondence of subtypes in our dataset with those in Allen Brain Institute datasets in fig. S3). The subpopulations were annotated in a hierarchical manner, similar as before (*30*), with the medium resolution denoting neuronal subfamilies and high resolution representing specific subtypes (table S3). At the highest resolution, we distinguished a total of 15 principal neuron and 20 GABAergic interneuron transcriptomic subtypes (Fig. 1, B to D; fig. S4, A to D; and table S3). Each subtype incorporated cells from multiple control and schizophrenia samples (except glial nuclei mostly derived from MB19, MB53, and MB51, explained further), and every subtype was present in at least 70% of the samples (fig. S4, D to G). Age, PMI, sex, disease conditions, and other sample characteristics were evenly distributed across uniform manifold approximation and projections (UMAPs) (fig. S5; only the glia batch originating from MB19, MB51, and MB53 was apparent). Fluorescence-activated nucleus sorting (FANS) separation of neuronal nuclei was very efficient, with 94% of nuclei in the dataset being neuronal and only 6% derived from glia (Fig. 1C), where glial nuclei are smaller and express less genes [fig. S4A and as reported previously (*32*)]. Because our study was focused on neurons, glial nuclei were excluded from the subsequent analyses. The subtype "Other" represented nuclei of lower quality (fig. S4, A to C) that lacked distinct subtype identity and thus were also excluded from further analysis. To predict layer-specific distributions of different neuronal types in our dataset, we aligned the analyzed nuclei with recent datasets (*32*, *33*), in which layer positions were determined experimentally by cortical layer microdissections before nucleus isolations and sequencing (Fig. 1E).

To characterize schizophrenia-related differences in the DLPFC, we first examined whether the composition of the cortex was altered in schizophrenia patients. Analysis of normalized cell density on the joint UMAP embedding (Fig. 2A) and direct comparison of cell proportions (fig. S6, A and B; for exact numbers of fraction of nuclei for each neuronal family/subtype, see table S4) showed a general decrease in GABAergic interneurons in schizophrenia, affecting subtypes from all families, in particular those belonging to PVALB, SST, and VIP. This was countered by an increase in the fraction of principal neurons belonging to L2_3_CUX2 family and to L4_5_FEZF2_LRRK1 subtype (Fig. 2A and fig. S6, A and B). As changes in proportion of one subtype could potentially skew the representation of other subtypes, we applied compositional data analysis techniques

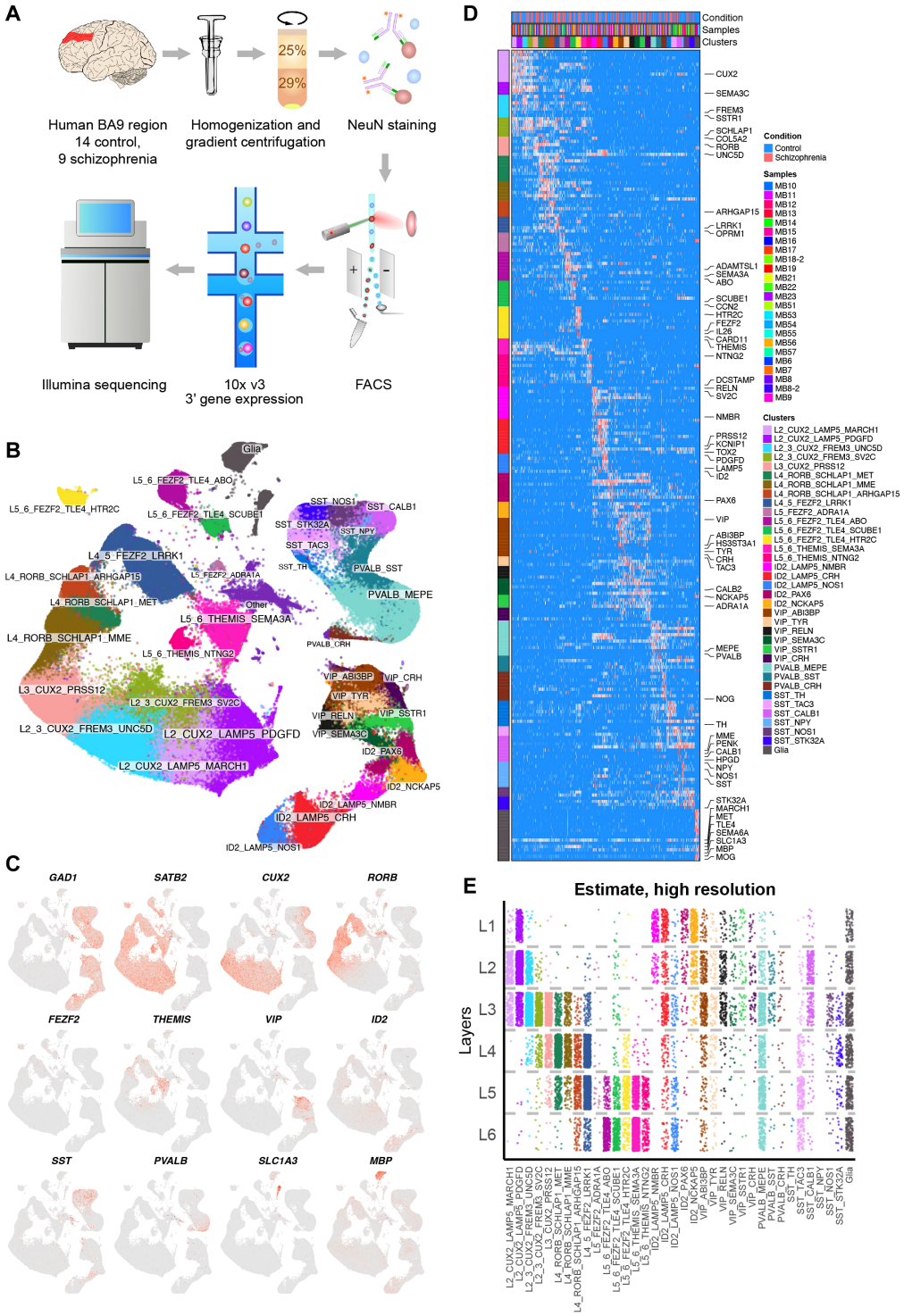

Fig. 1. snRNA-seq analysis of the DLPFC from patients with schizophrenia and matched controls. (**A**) Experimental design of the snRNA-seq measurements. FACS, fluorescence-activated cell sorting. (**B**) UMAP representation of the measured nuclei, colored by subtypes. (**C**) Expression of marker genes for major cortical cell types, visualized on the UMAP embedding: GABAergic interneurons, principal neurons, and glia; additional markers distinguish families of GABAergic interneurons and principal neurons. (**D**) Heatmap showing expression of markers for specific neuronal subtypes. (**E**) Estimated cortical layer positions of the neuronal subtypes. These are predictions based on Allen Institute data (*32*, *33*) with manual cortical layer microdissections before nuclei isolation and sequencing. Because of manual layer dissections, small degree of mispositioning of subtypes (e.g., principal neurons in layer 1) is expected.

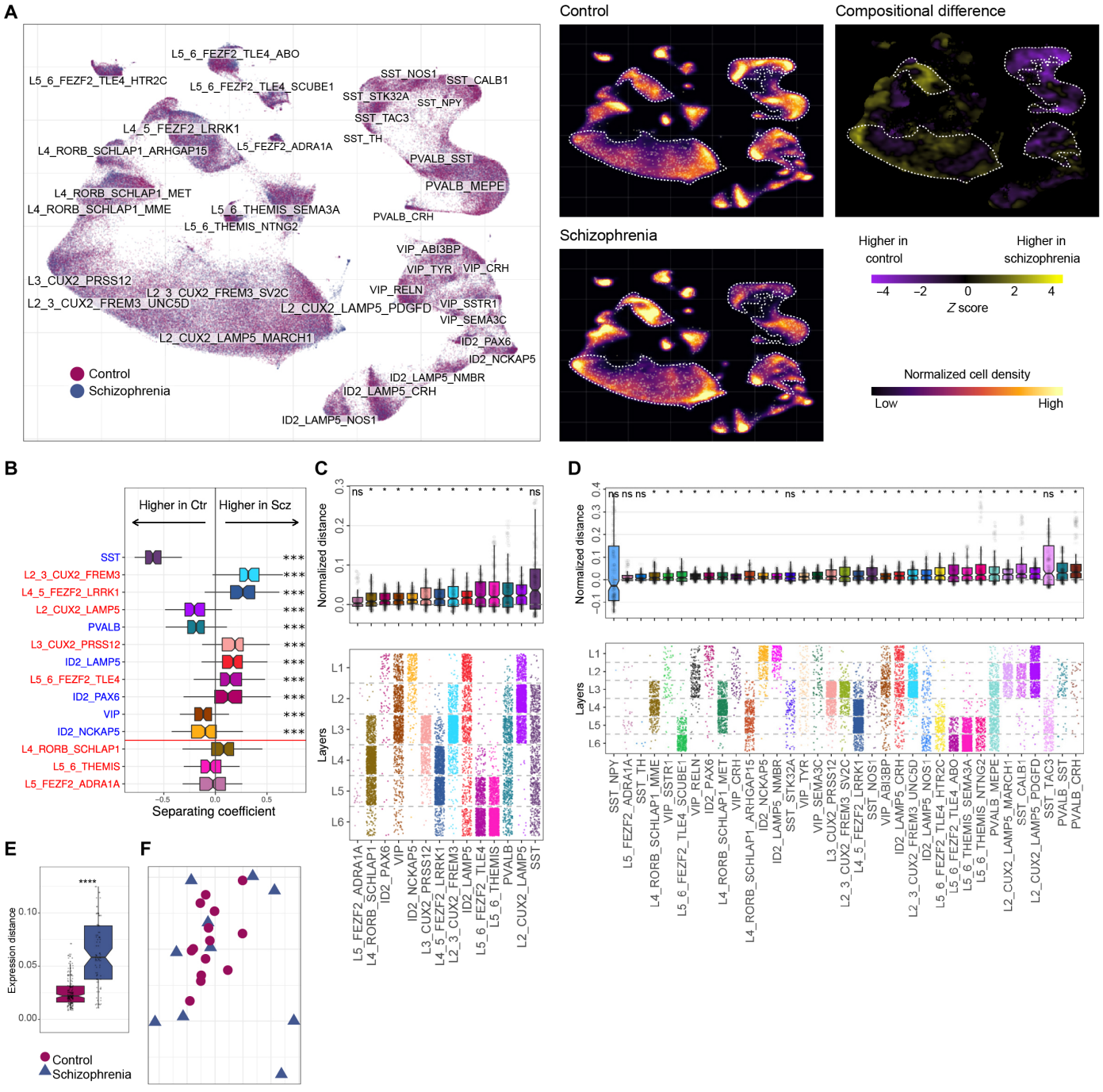

Fig. 2. Compositional and transcriptomic changes in the cortex of patients with schizophrenia. (**A**) Cell density differences between schizophrenia and control groups analyzed using UMAP embedding. Left: Visualization of control and schizophrenia cells. Middle: Cell density visualized from the control and schizophrenia samples, using UMAP embedding. Right: Statistical assessment of the cell density differences. Student's *t* test was used, visualized as a *z* score. (**B**) Change in neuronal composition evaluated by compositional data analysis. Top cell types distinguishing composition of control and schizophrenia samples are shown. The *x* axis indicates the separating coefficient for each cell type, with the positive values corresponding to neurons with increased abundance in schizophrenia and negative values to decreased abundance. The boxplots and individual data points show uncertainty based on bootstrap resampling of samples and cells (for full plot, see fig. S6C). Red line represents cutoff for significance of adjusted (by the Benjamini-Hochberg method) *P* values (significant cell types are above the line). ****P* = 0.0001 to 0.001. (**C** and **D**) Boxplots showing the magnitude of transcriptional change between control and schizophrenia states for medium-resolution (C) and high-resolution (D) annotations. The magnitude is assessed on the basis of a Pearson linear correlation coefficient, normalized by the medium variation within control and schizophrenia groups (see Materials and Methods). The cell types are ordered on the basis of the mean distance, with the most affected cell types shown on the right. The distribution here arises as a result of comparisons of different pairs of patients/controls. The lower panels show the predicted cortical layer positions. Multiple correction was done by Benjamini-Hochberg. **P* = 0.01 to 0.05. ns, not significant. (**E**) Boxplots showing interindividual gene expression distances (based on Pearson correlation) within control and schizophrenia samples, averaged across all neuronal cell types. *****P* = 0.00001 to 0.0001. (**F**) Multidimensional scaling visualization of the similarity of gene expression between all samples, based on the distances shown in (E).

(*34*, *35*) to calculate robust estimates of compositional changes (see Materials and Methods). This analysis confirmed that schizophrenia was linked to a general increase in most subtypes of L2_3_CUX2 and L5_6_FEZF2 (that includes L4_5_FEZF2_LRRK1) families of principal neurons, and a decrease in several interneuron subtypes, most notable for those in SST and PVALB families (Fig. 2B and fig. S6C), which included subtypes localized in L2-L3 (such as SST_CALB1; fig. S6C). Last, to validate compositional changes in principal neurons by an independent dataset, we reanalyzed the largest bulk transcriptomic dataset of schizophrenia brains in the same region—the DLPFC (CommonMind: 353 schizophrenia and 501 control individuals) (*24*, *36*)—and performed deconvolution of neuronal subtypes based on their signatures from our dataset. Because of the complexity and the overlapping nature of transcriptomic signatures characterizing fine neuronal subtypes, such approach could be implemented only for families of principal neurons. Deconvolution confirmed that L2_3_CUX2 and L5_6_FEZF2 families have increased proportion in the DLPFC of schizophrenia patients (fig. S6D). Markers that were used for deconvolution were expressed similarly between control and schizophrenia conditions (fig. S6E).

Overall, several approaches led to consistent results for compositional changes of neuronal subtypes in the DLPFC of schizophrenia patients. Compositional data analysis, normalized cell density on UMAP, and the fraction of nuclei showed a decrease in SST and PVALB families of GABAergic neurons, with the most notable change in the upper-layer subtype of SST—SST_CALB1. In addition, an increase in abundance of upper-layer principal neurons was shown by compositional data analysis and normalized cell density on UMAP, and such increase was confirmed by an independent sample set from CommonMind using deconvolution.

We then examined the extent to which the transcriptional state of different neurons may be altered in schizophrenia. Using an expression distance measure based on the Pearson linear correlation, for each annotated type, we compared the distances between schizophrenia and control samples with the average distance observed within schizophrenia and controls. At medium resolution, L2_CUX2_LAMP5 subfamily of principal neurons and PVALB family of GABAergic interneurons showed the largest difference between control and schizophrenia transcriptomes, based on normalized distance in gene expression between conditions for each subtype (Fig. 2C). When zooming in further, five individual subtypes with the largest expression shifts belonged to neuronal subtypes from the upper layers—PVALB_CRH, PVALB_SST, L2_CUX2_LAMP5_PDGFD, SST_CALB1, and L2_CUX2_LAMP5_MARCH1 (Fig. 2D).

Schizophrenia is a spectrum disorder with expected high interpatient variability (*37*). Thus, we examined the magnitude of transcriptional differences observed within the control and schizophrenia groups. We found that schizophrenia patients showed significantly greater interindividual expression variability (Fig. 2E), a trend that was pronounced across all neuronal subtypes (fig. S7A). Consistently, when visualizing the distances between samples using multidimensional scaling, we found that while controls were grouped closer together, the schizophrenia samples were scattered in different directions (Fig. 2F). Because large within-group distances may occlude the extent to which different neuronal types are affected by schizophrenia, we repeated the analysis of transcriptional shift magnitudes using a more complex distance measure that quantifies changes occurring only along the direction of the overall difference between schizophrenia and control states (see Materials and Methods). Specifically, for each cell type, we first determined a consensus pattern of expression differences between schizophrenia and controls. The distances between any pair of schizophrenia and control samples were then quantified by projecting the samples onto that consensus axis and normalized by the distances expected from randomized assignment of samples to the control and schizophrenia groups. Such analysis revealed lack of significant expression shifts along the "common" direction for any neuronal subtype in schizophrenia (fig. S7, B and C). Thus, lack of common expression shifts and extension of schizophrenia samples in multiple directions on multidimensional scaling plots suggest that the diversity of schizophrenia phenotypes might be grounded in the diversity of transcriptomic changes in neuronal subtypes.

Overall, the strongest effect of schizophrenia on compositional and transcriptomic changes was attributed to subtypes of principal neurons and GABAergic interneurons in L2-L3 of the DLPFC. There is a large body of evidence showing extensive evolution of L2-L3 along the rodent-primate-human axis, mainly for principal neurons (*38*–*40*). As evolutionary divergence of interneurons is not well understood, we quantified the interspecies expression distances based on a recent alignment of human, marmoset, and mouse motor cortex (*41*). The analysis showed that ID2 and PVALB subtypes in the L2-L3 region have the highest expression divergence in humans (fig. S7, D and E). Thus, the hotspot of changes in L2-L3 subtypes correlates with the position of the evolutionarily most diverged human neuronal subtypes.

Histological analysis revealed density decrease of interneuron subtypes in the upper cortical layers in schizophrenia

The largest compositional and transcriptomic changes in schizophrenia were attributed to subtypes of GABAergic interneurons and principal neurons in upper layers 2 and 3 of the DLPFC. To further investigate this and attempt to bridge previous neurohistological studies with our transcriptomic findings, we performed immunohistochemical (IHC) characterization of different families of GABAergic interneurons across all cortical layers in paraffin-embedded brain samples, including cases analyzed by snRNA-seq (Fig. 3A and table S5). We labeled calretinin-expressing (CR^+; encoded by the gene *CALB2*) GABAergic interneurons, the most enriched interneuron marker in upper cortical layers in human brain (*42*), and PV-expressing GABA interneurons (PV^+; encoded by the gene *PVALB*) and applied the general principal cell marker SMI 31.1 (the protein product of *NEFH* and *NEFM* genes) in 10 schizophrenia and 10 control samples. Calbindin (CB^+; encoded by the gene *CALB1*) and neuropeptide Y (NPY^+; encoded by the gene *NPY*) GABAergic interneurons were analyzed in a subset of six schizophrenia and six control samples. We applied Nissl staining to this subset of samples and calculated total neuronal density in the layers of the DLPFC.

On the basis of our transcriptomic data, cells expressing CR mRNA represent all VIP subtypes and two ID2 subtypes: ID2_NCKAP5 and ID2_PAX6 (Fig. 1D). While the density of CR^+ interneurons in L1 and L3-L6 was similar between the conditions, we found a significant decrease explicitly in L2 in schizophrenia ($P = 0.0028$, Bonferroni-corrected; Fig. 3, B and C, and table S5F). A conspicuous "L2 low CR phenotype" was found in 50% of cases with schizophrenia. The lower density of CR^+ neurons measured in sections from patients with schizophrenia was most probably not due to any volumetric differences as cortical widths were highly similar in the diagnostic groups

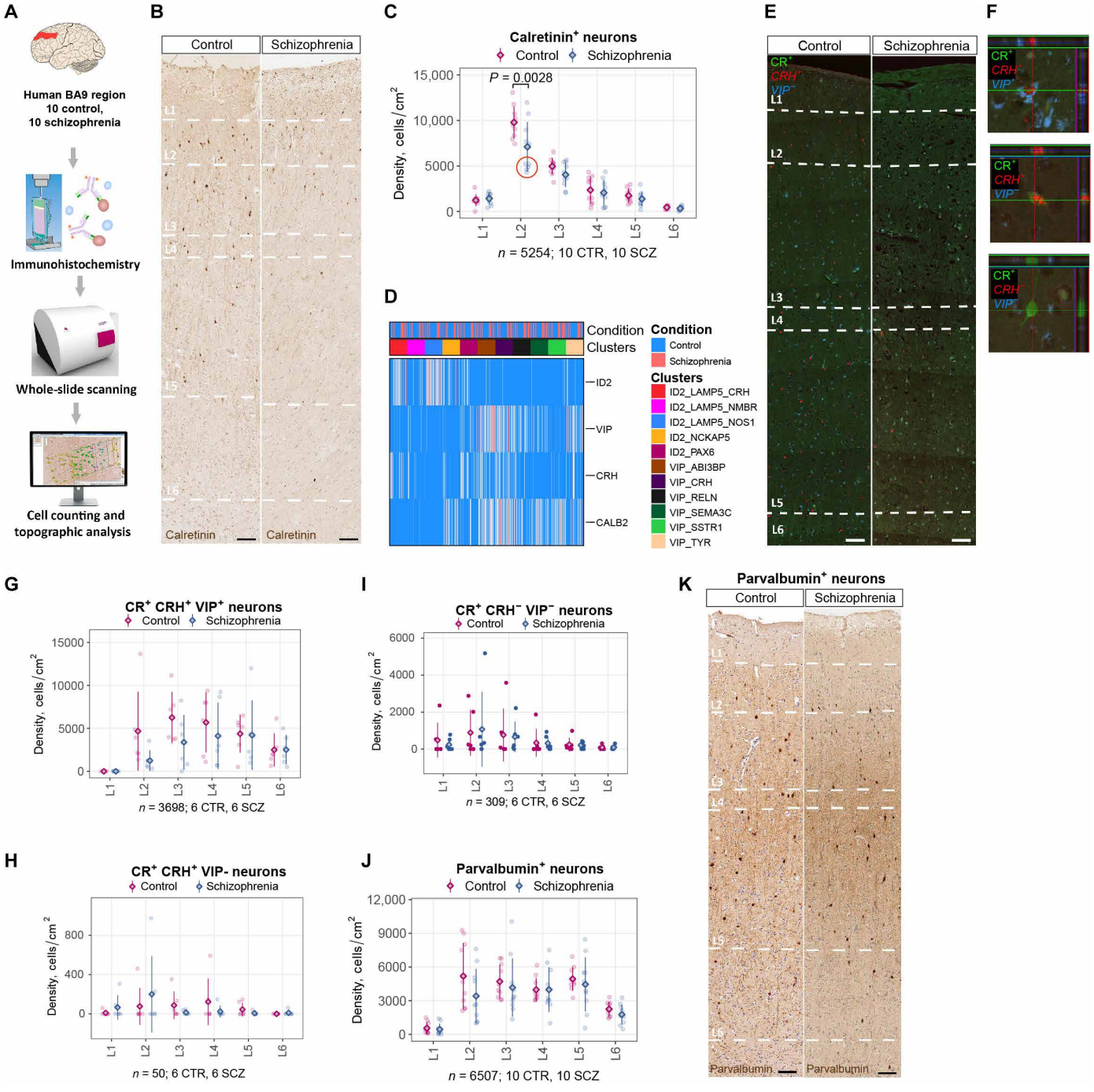

Fig. 3. Changes in density and distribution of CR$^+$, PV$^+$, VIP, and ID2 interneuron subtypes in the cortex of patients with schizophrenia. (**A**) Experimental scheme for immunohistochemical (IHC) analysis. (**B** and **C**) Representative images and layer-wise IHC quantification of CR$^+$ neurons in the DLPFC in patients with schizophrenia (SCZ) and control individuals (CTR); linear mixed model analysis with Bonferroni multiple comparison correction. Scale bars, 100 μm. (**D**) Heatmap showing expression of major markers for subgrouping of ID2 and VIP subtypes of GABAergic interneurons. (**E** and **F**) Overview of simultaneous CR IHC and smFISH of VIP and CRH mRNAs, and representative confocal images for three subgroups of ID2 and VIP subtypes that could be distinguished on the basis of triple CR/VIP/CRH labeling in L2 DLPFC. Scale bars, 100 μm. (**G** to **I**) Quantification of density for CR$^+$/VIP$^+$/CRH$^+$ (VIP_CRH, VIP_ABI3BP, and VIP_TYR), CR$^+$/VIP$^-$/CRH$^+$ (ID2_PAX6), and CR$^+$/VIP$^-$/CRH$^-$ (ID2_NCKAP5 and VIP_SSTR1) subgroups of ID2 and VIP subtypes; linear mixed model analysis with Bonferroni multiple comparison correction. (**J** and **K**) Representative images and layer-wise quantification of PV$^+$ neurons in the DLPFC in patients with schizophrenia and control subjects; linear mixed model analysis with Bonferroni multiple comparison correction. Scale bars, 100 μm. Diamonds on all plots represent means; error bars, ±SD.

(control: 2611 ± 308 μm, schizophrenia: 2613 ± 274 μm; table S5C). No statistically significant interaction between CR^+ density and PMI, age, or gender was detected. Diameters of CR^+ cells did not differ significantly in the diagnostic groups (table S5C). Furthermore, there was no indication for CR protein-content changes in CR^+ neurons in schizophrenia based on the labeling intensity of CR^+ neurons or subtype-specific gene expression data (fig. S7F).

To distinguish VIP and ID2 subtypes and potentially identify which of these might account for the observed CR^+ density reduction in the schizophrenic DLPFC, we used single-molecule fluorescence in situ hybridization (smFISH) and implemented a set of the following markers based on transcriptomic data: CR, VIP, and corticotropin-releasing hormone (CRH). We measured the density of $CR^+/VIP^+/CRH^+$ cells, which represent VIP_CRH, VIP_ABI3BP, and VIP_TYR subtypes; $CR^+/VIP^-/CRH^+$ cells, which represent the ID2_PAX6 subtype; and $CR^+/VIP^-/CRH^-$ cells, which represent ID2_NCKAP5 and VIP_SSTR1 subtypes (Fig. 3, D to F). We confirmed that all of these subpopulations were most abundant in L2-L3. The triple-positive $CR^+/VIP^+/CRH^+$ subtype showed reduced density in L2 and in L3, suggesting this subtype of CR interneurons being the most affected (Fig. 3G). However, these changes were not statistically significant when applying Bonferroni correction for multiple comparisons (table S5F).

PV^+ and CB^+ GABAergic interneurons also had subtypes with large compositional and transcriptomic changes in the snRNA-seq analysis. Although our histological analysis showed a marked reduction in the density of PV^+ interneurons in L2 in schizophrenia (Fig. 3, J and K) and a visible decrease in CB^+ interneuron density in L2 in schizophrenia (Fig. 4, A and B), the PMI showed a significant confounding effect in both cases ($P = 8.3 \times 10^{-7}$ and 4.6×10^{-3}, respectively; table S5F). This might be due to inclusion of some high PMI samples in histological analyses, due to the lack of low PMI samples, whereas snRNA-seq analysis was done exclusively on low PMI samples. The histological analysis of NPY^+ neurons (representing mainly the SST_NPY transcriptomic subtype) revealed no significant layer-specific differences between diagnostic groups (Fig. 4, C and D, and table S5G). Labeling for Nissl and SMI31.1 showed no statistically significant density reduction in total neuronal or principal neuronal densities, respectively, in any cortical layer (Fig. 4, E to H).

Major transcriptomic changes across cortical layers are associated with neurotransmission, energy metabolism, and protein homeostasis

To gain further insights into the transcriptomic changes in schizophrenia, we calculated differentially expressed genes (DEGs) for each subtype between schizophrenia and control samples (figs. S8 and S9; complete data on DE for each subtype with all statistical information are in Supplementary Dataset Table 1, https://doi.org/10.5281/zenodo.5810785). Concordant with the snRNA-seq results above, higher fraction of DEGs (estimated while controlling for the differences in the number of the measured nuclei) was dysregulated in the upper cortical layer subtypes (Fig. 5A).

To validate neuronal subtype-specific DEGs from snRNA-seq data, we selected a gene coding for neurotransmission protein, *CHRFAM7A*, that was prominently expressed across CR^+ neuronal subtypes and exhibited robust down-regulation in schizophrenia (Fig. 5B). CHRFAM7A is a human-specific fusion protein that has acetylcholine receptor properties and was proposed to have a unique role in schizophrenia (*43*). Using smFISH, we examined a subset of schizophrenia and control DLPFC sections ($n = 3$ versus 3) to validate the changes in expression of *CHRFAM7A* in CR^+ cells in patients with schizophrenia. The ratio of L2 CR^+*CHRFAM7*$^+$ to all L2 CR^+ neurons was decreased by 18% in patients with schizophrenia. Furthermore, expression levels of *CHRFAM7* in L2 CR^+ neurons were reduced in patients with schizophrenia by 77% (Fig. 5, C and D). Thus, smFISH analysis further supports our snRNA-seq identification of transcriptomic changes in the cortex of patients with schizophrenia.

Although our samples were well balanced with regard of potential confounders (figs. S1 and S4), imbalance of medication in the form of neuroleptic drugs could not be avoided, as the use of antipsychotics is standard among the schizophrenia patients and is not encountered in control individuals. To make sure that the patterns of DE are not associated with this medication regiment, we analyzed two bulk RNA datasets of the DLPFC: one large dataset consisting of ~150 human postmortem samples from antipsychotic-positive and antipsychotic-negative patients (*44*), and another consisting of ~35 rhesus macaque samples that were treated with the antipsychotic clozapine or haloperidol or with placebo (*36*). We overlapped human antipsychotic-associated or macaque drug treatment–associated DEGs with DEGs between control and schizophrenia samples either for all excitatory or inhibitory neurons or for each neuronal subtype in our dataset. We found that the resulting overlap was negligible (Fig. 5, E to G), indicating that the DEGs distinguishing schizophrenia patients from controls were likely associated with schizophrenia and not with the antipsychotic treatment.

To explore pathways that might underlie schizophrenia-related changes in neuronal function, we extracted top up/down-regulated genes for each subtype and calculated enrichment for Gene Ontology (GO) terms (Supplementary Dataset Table 2, https://doi.org/10.5281/zenodo.5810785). The most significant GO terms down-regulated were related to energy metabolism and protein biogenesis and localization [see top 3 GO terms per subtype (or fewer if there are <3 significant GO terms) in Fig. 5H and the complete list in fig. S10]. In contrast, up-regulated genes were enriched for functionally relevant pathways, which were related to neurotransmission, plasticity, and developmental processes [see top 3 GO terms per subtype (or fewer if there are <3 significant GO terms) in Fig. 5I and the complete list in fig. S11]. Schizophrenia-induced down-regulation of energy metabolism and protein biogenesis pathways and up-regulation of neurotransmission and plasticity pathways point to the impairment of energy supply and protein synthesis in affected neuronal subtypes and aberrant activity of neuronal networks in schizophrenia. We noted that the up-regulation of neurotransmission and plasticity GO terms and down-regulation of energy metabolism and protein synthesis GO terms similarly affected a large group of neuronal subtypes, mainly upper-layer GABAergic interneurons and L2_3_CUX2 and L5_6_FEZF2 families of principal neurons (fig. S12, A and B, for families and fig. S12, C and D, for subtypes). Clustering of GO terms by their enrichment level in each of the subtypes revealed groups of subtypes with similar enrichment patterns, which suggest them being in the same neuronal network. Thus, there were some upper layer–specific networks, for instance, upper-layer VIP_ABI3BP GABAergic interneurons clustered with L2_3_CUX2_LAMP5_PDGFD (fig. S12E) and upper-layer SST_CALB1 clustered with L2_3_CUX2_LAMP5_PDGFD, upper-layer PVALB_SST with L2_3_CUX2_FREM3_SV2C and L2_3_CUX2_FREM3_UNC5D, and upper-layer PVALB_CRH with ID2_LAMP5_NOS1 (fig. S12F).

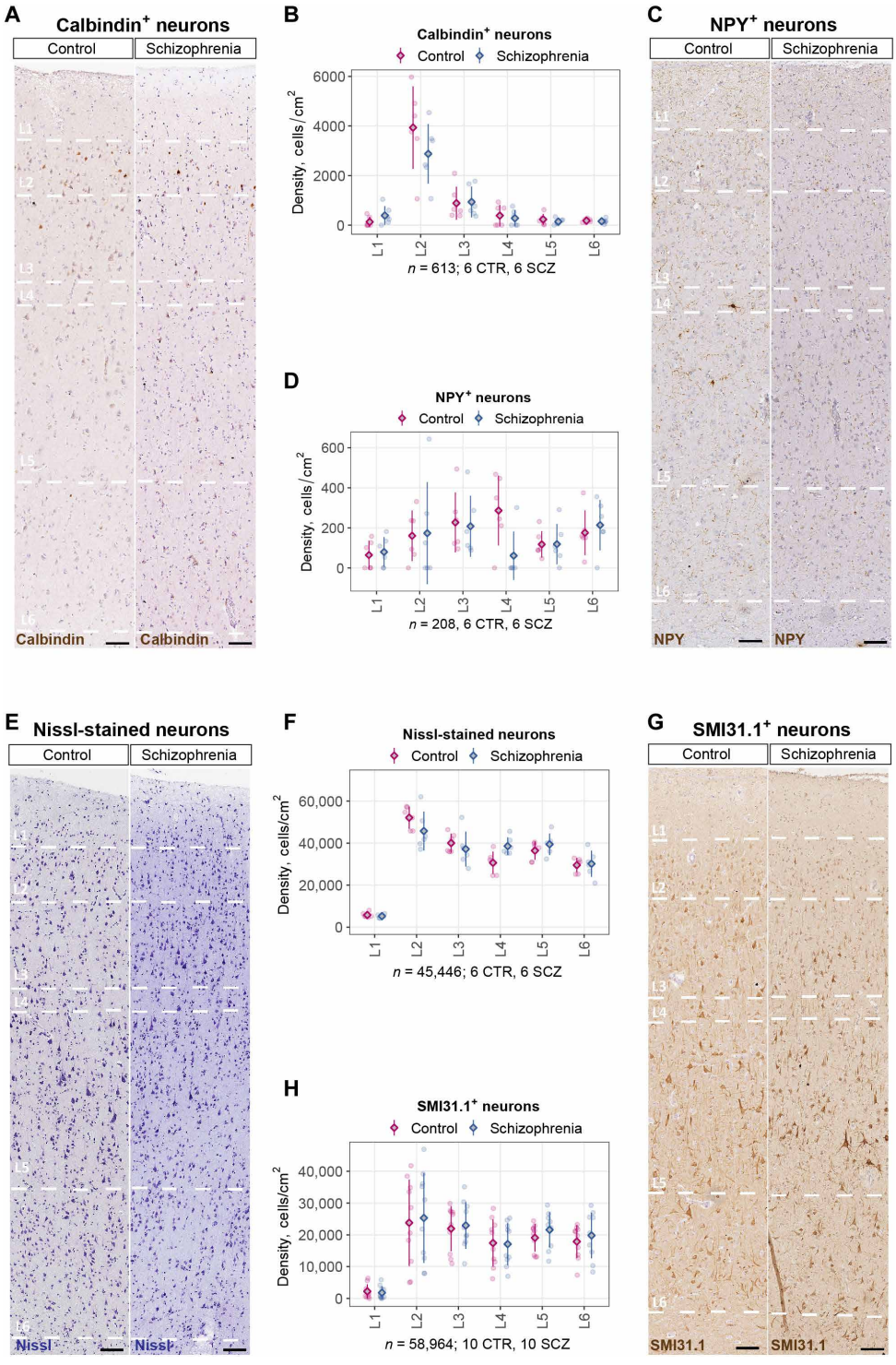

Fig. 4. Changes in density and distribution of CB$^+$and NPY$^+$ interneurons and excitatory neurons in the DLPFC in schizophrenia. (**A** and **B**) Representative immunohistochemical (IHC) images and layer-wise quantification of GABAergic interneurons that express CB in the DLPFC in patients with schizophrenia and control subjects. (**C** and **D**) Representative IHC images and layer-wise quantification of GABAergic interneurons that express NPY neurons in the DLPFC in patients with schizophrenia and control subjects. (**E** and **F**) Representative IHC images and layer-wise quantification of Nissl-labeled neurons in the DLPFC in patients with schizophrenia and control subjects. (**G** and **H**) Representative IHC images and layer-wise quantification of principal neurons labeled by SMI31.1 in the DLPFC in patients with schizophrenia and control subjects. Diamonds on all plots represent means; error bars, ±SD. Analysis of cell densities on (B), (D), (F), and (H) was done using linear mixed model analysis with Bonferroni multiple comparison correction.

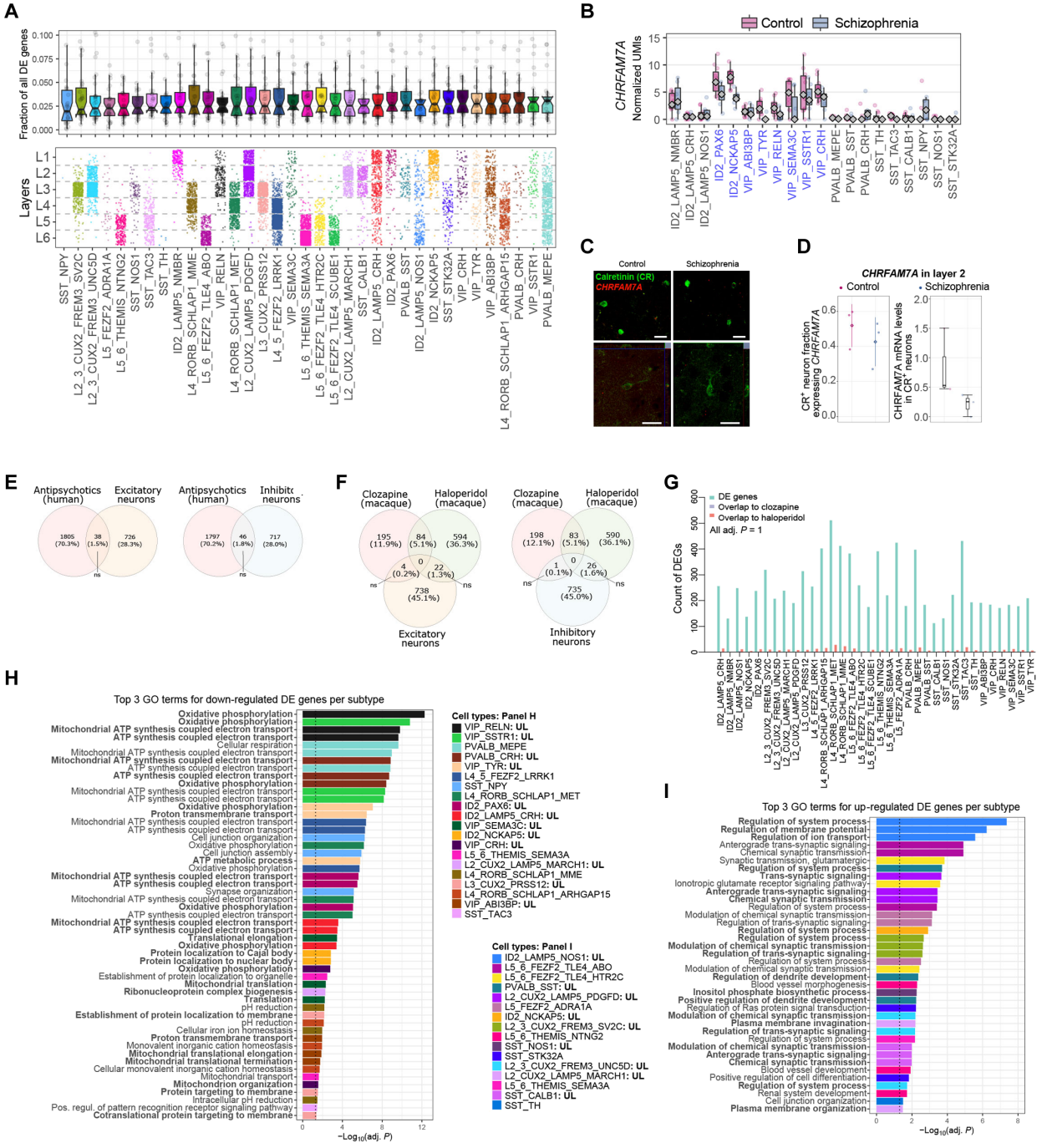

Fig. 5. Schizophrenia-associated changes in the DEGs and pathways. (**A**) Fraction of all DEGs with predicted cortical layer positions below. Line inside the box represents median, and lower and upper hinges of the box correspond to the first and third quartiles. Upper and lower whiskers correspond to the smallest and the largest values. (**B**) Expression levels of *CHRFAM7A* across neuronal subtypes in the DLPFC identified by snRNA-seq. CR^+ subtypes are highlighted in blue; *P* values were estimated by Wald test in DESeq2, multiple comparison correction by the Benjamini-Hochberg method. Diamond represents median. (**C**) Representative images for detection of CHRFAM7A mRNA in L2 CR^+ neurons of schizophrenia and control subjects. Scale bars, 20 μm. (**D**) Quantification of proportion of L2 CR^+ neurons that colocalize with CHRFAM7A mRNA in schizophrenia and control DLPFC ($n = 3$ control + 3 schizophrenia, means ± SD) and CHRFAM7A mRNA levels in L2 CR^+ neurons. (**E**) DEGs were determined for antipsychotic-positive (100) and antipsychotic-negative (47) bulk RNA-seq samples for the DLPFC of schizophrenia patients. Overlap between antipsychotic-associated DEGs and DEGs for control versus schizophrenia in our snRNA-seq dataset was identified by hypergeometric test. Benjamini-Hochberg–adjusted *P* values. (**F** and **G**) DEGs were determined for placebo versus haloperidol/clozapine bulk RNA-seq samples for the DLPFC of rhesus macaque ($n = 34$). Overlap between drug treatment DEGs and DEGs for control versus schizophrenia in our snRNA-seq dataset was identified by hypergeometric test. Benjamini-Hochberg–adjusted *P* values. (**H** and **I**) List of GO terms significantly enriched in the set of top down- and up-regulated genes in the neuronal subtypes from schizophrenia DLPFC, compared to controls. Top 3 GO terms by adjusted *P* value per each cell type are shown. Colored by neuronal subtype. UL, upper layers. UL GO terms are in bold. Bonferroni-adjusted *P* values are shown. Dotted line represents *P* value significance cutoff. The full list of significant GO terms is in figs. S10 and S11.

In addition, cross-layer networks were also detected, such as a large cluster of PVALB, ID2, and VIP GABAergic neurons with L4_5 principal neuron subtypes (fig. S12E). These results highlight transcriptional disturbances across different neuronal subtypes that are potentially organized in local upper-layer networks or longer-range networks spanning upper and lower layers in the human DLPFC. These cortical network disturbances most probably contribute to neuropsychiatric symptoms of schizophrenia.

In addition, we checked the expression of neurotransmitter receptors that have been proposed to contribute to schizophrenia-associated phenotypes or to be targets of frontline antipsychotic drugs (*45*, *46*)—dopamine receptor *DRD2*, GABA receptor *GABRA1*, kainate-type glutamate receptor *GRIK3*, *N*-methyl-D-aspartate (NMDA)–type glutamate receptors *GRIN2A* and *GRIN2C*, and oxytocin receptor *OXTR* (fig. S12G). Among these, *GABRA1* expression was decreased in SST_TAC3, SST_STK32A, and PVALB_CRH; *GRIN2A* expression was down-regulated in PVALB_CRH, while decreased *OXTR* expression was detected in SST_NPY (adjusted for multiple hypotheses) (fig. S12G). We also noted that these receptor genes were expressed from few to several neuronal subtypes. Modulation of these target receptors has a beneficial effect on target neuronal subtypes misexpressing these receptors in schizophrenia. However, undirected delivery of modulators can potentially influence other nonaffected neuronal subtypes, further increasing the complexity of neuronal perturbations in schizophrenia.

Footprint-based analysis of transcription factor enrichment identified schizophrenia-related transcriptional regulators

To infer transcription factor activity from snRNA-seq data, we used the DEGs between schizophrenia and control samples as the potential transcription factor targets and the regulon database obtained from DoRothEA (*47*). We performed enriched regulon analysis using the aREA algorithm, which is implemented within the VIPER package (*48*) using the *z* scores from DEGs. We estimated the expression of 267 unique transcription factors across all cell types, which were further analyzed with hierarchical clustering to identify differentially enriched regulators associated with schizophrenia (Fig. 6, A and B; see fig. S13 for the complete heatmap). Our analysis revealed a number of transcription factors that had been already linked to schizophrenia by genome-wide association study (GWAS) analyses, including *TCF4*, *PRDM14*, *ASCL1*, *POU5F1*, *TEAD1*, *ZEB2*, and *FOXP1* (*49*–*52*). Some of the identified factors with the highest and lowest enrichment scores (*TCF4*, *ASCL1*, *ZEB2*, *HIF1A*, and *LHX2*) were highlighted in the study of another area of the prefrontal cortex, BA10, of patients with schizophrenia by snRNA-seq (*53*), thus validating our data. The basic helix-loop-helix transcription factors TCF4 and ASCL1 are considered to be important susceptibility factors in schizophrenia involved in cortical neurogenesis, maturation, and neuronal migration (*54*, *55*), and both of them were positively enriched in a cluster of upper and lower cortical layer subtypes (Fig. 6B). In addition, clusters of SST interneuron subtypes and upper-layer L2_3_CUX2 principal neuron subtypes showed negative enrichment in HIF1A, a hypoxia factor connected to impairments in brain morphology and abnormal nervous system development (*54*), and two factors important for lipid biosynthesis and antipsychotic response, SREBF1 and SREBF2 (*56*) (Fig. 6A). Moreover, SST neurons showed an increase in ZEB2 and FOXP1, both transcription factors identified by GWASs associated with structural brain abnormalities (*57*–*59*). Overall, the analysis of transcription factor networks confirms the relevance of the identified pathways to neurodevelopmental impairments and schizophrenia. Misexpression of transcriptional regulators could contribute to the perturbations of neuronal circuits in schizophrenia.

Integration of single-nucleus transcriptomics and genetics data supports relevance of transcriptomic changes to schizophrenia

To provide further support for relevance of transcriptomic changes identified in our study to schizophrenia, we integrated snRNA-seq data with several datasets containing genes previously associated with schizophrenia and other mental disorders. We first preformed hypergeometric testing to identify significant overlaps between DEGs in our dataset with genes relevant for schizophrenia from the DisGeNET database (*60*). This analysis identified SST GABAergic neurons, upper-layer subtypes of PVALB and VIP GABAergic neurons, and principal neurons belonging mainly to L2_3_CUX and L5_6_FEZF2 families as the subtypes with the most significant enrichment of DEGs in schizophrenia-linked genes (Fig. 6C). We also performed such analysis for autism spectrum disorder genes from the Simons Foundation Autism Research Initiative (SFARI) database, which showed similar results (Fig. 6D), emphasizing commonalities in neuronal network impairments between schizophrenia and autism spectrum disorder. Integration of our snRNA-seq data with the largest schizophrenia GWAS dataset (*61*) selectively identified the L2_CUX2_LAMP5_PDGFD subtype in the upper cortical layers as having enrichment in schizophrenia GWAS genes (Fig. 6E). Overall, the genetic data strongly correlate with the snRNA-seq analysis results, thus further indicating the relevance of the changes identified in our study to impairments in brain function associated with mental disorders.

Spatial transcriptomics confirmed perturbations in the upper cortical layers

To enhance the spatial resolution and further validate schizophrenia-related transcriptomic and compositional alterations in the DLPFC, we used the Visium spatial transcriptomics assay (Fig. 7A). We analyzed seven schizophrenia and seven control donors previously included in our snRNA-seq and histology cohorts (tables S1, S2, and S6). Changes in gene expression identified by spatial transcriptomics overlapped with previously detected gene expression changes in snRNA-seq data, in particular, in the upper layers (Fig. 7B; fig. S12, H and I; and Supplementary Dataset Tables 3 and 4, https://doi.org/10.5281/zenodo.5810785). The overlapping GO terms fall within important groups of neurotransmission, synapse organization, and metabolism, thus highlighting physiologically relevant commonalities of the spatial and single-nucleus transcriptomic readouts. We further analyzed DEGs identified by spatial transcriptomics and noticed a hotspot of transcriptomic changes in the upper layers of the cortex, showing GO terms related to cognition, neurodevelopment, and neurotransmission, whereas differential pathways in the lower layers were much less prominent (Fig. 7, C and D; fig. S12, J and K; and Supplementary Dataset Table 4, https://doi.org/10.5281/zenodo.5810785), which was consistent with our snRNA-seq results. We also noted possible perturbations of glia, because in the spatial analysis all cell types of the DLPFC are present (Supplementary Dataset Table 4, https://doi.org/10.5281/zenodo.5810785), giving us even further insights into the high complexity of schizophrenia at the spatial tissue level.

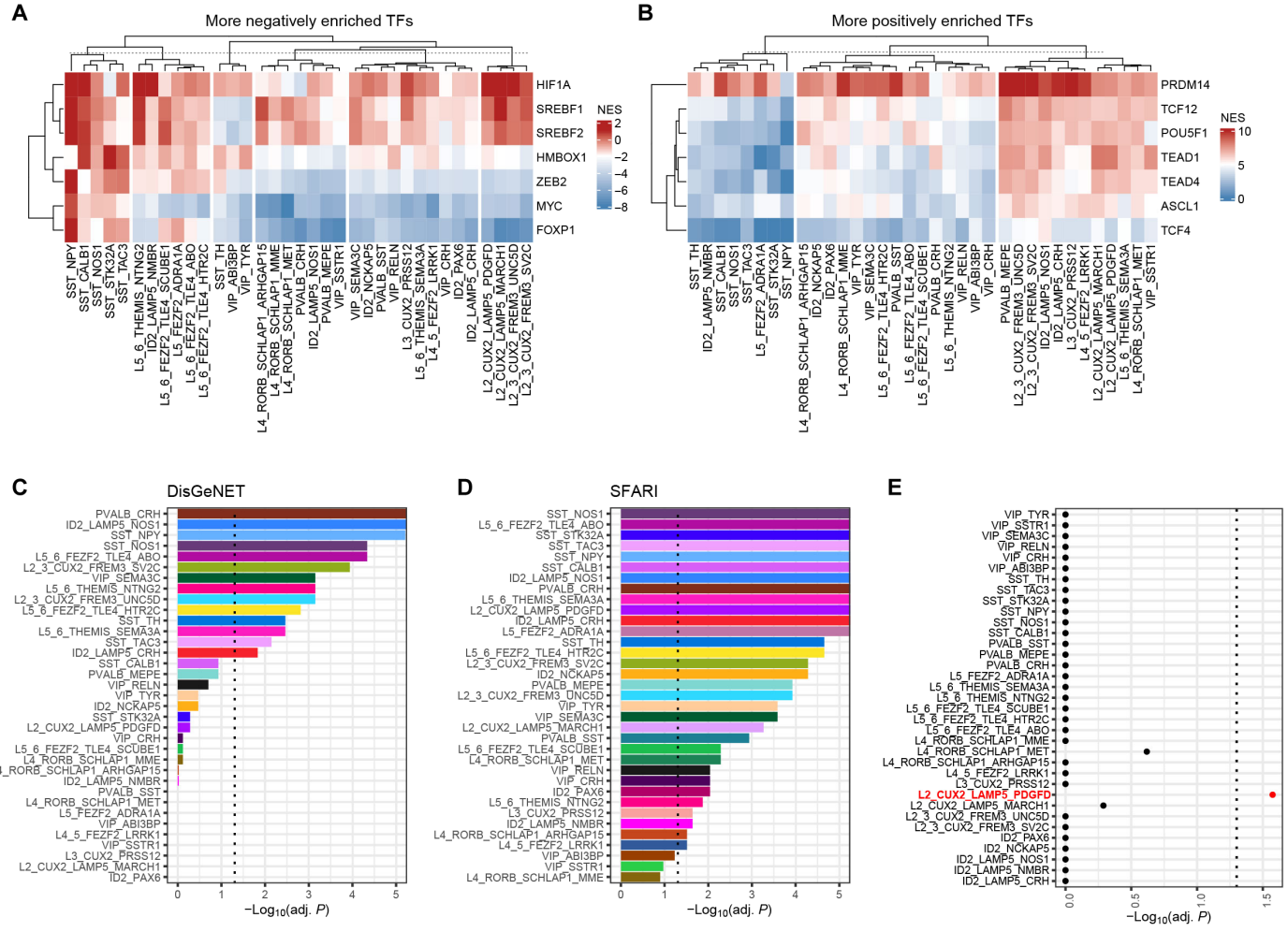

Fig. 6. Transcription factor networks in schizophrenia and enrichment of DEGs in genetic association with schizophrenia. (**A** and **B**) Transcription factor (TF) enrichment in DEG genes was estimated based on the *z* score of the DEGs and was normalized for the purpose of hierarchical clustering. Overall, expression of 267 unique transcription factors across all cell types was estimated, which were further analyzed with hierarchical clustering to identify differentially enriched regulators associated with schizophrenia (see fig. S13 for the complete heatmap). NES, Normalized enrichment score. (**C** and **D**) Hypergeometric testing to identify significant overlap between DEGs in our dataset with genes relevant for schizophrenia from the DisGeNET database (*60*) and from the SFARI database. Black dotted line indicates *P* value cutoff. *P* values were adjusted using Bonferroni correction. (**E**) Linkage disequilibrium score regression analysis to estimate correlation between DEGs and with the largest schizophrenia GWAS dataset (*61*). L2_CUX2_LAMP5_PDGFD subtype (marked in red) showed significant correlation after adjusting *P* value by Bonferroni correction. Dotted line, significance cutoff.

Spatial analysis confirmed our earlier estimates of layer-specific distribution of principal neurons and preferential localization of GABAergic interneurons (Fig. 7E and fig. S14). We validated compositional changes of a subset of principal and GABAergic neurons with a larger effect on the upper cortical layers compared to the lower layers (Fig. 7F). These findings further substantiate our previous snRNA-seq and histological observations of the perturbation of upper cortical layer neurons in schizophrenia. The overview of our findings summarizing the major transcriptomic and compositional changes in the DLPFC in schizophrenia is shown in Table 1.

DISCUSSION

We present a comprehensive study identifying cortical neuronal subtypes affected in schizophrenia. We detected differential changes in neuronal subtypes deriving mainly from the upper cortical layers. Combining all of the assessments of neuronal subtypes performed in this study, we conclude that subtypes of GABAergic interneurons and principal neurons in the upper cortical layers have the largest changes in schizophrenia, and thus are likely to have the strongest contribution to schizophrenia phenotype. Such hotspot of changes in layer 2 and 3 subtypes may underlie the human nature of schizophrenia, because upper layers are the most expanded cortical layers in the human cortex (*38*) and have increased morphological, transcriptomic, and functional complexity along the rodent-primate-human axis (*39*, *40*). Accordingly, our data and earlier studies (*62*) show that layers 2 and 3 of the human cortex exhibit the highest complexity of GABAergic interneurons, which also have the largest divergence from their rodent and monkey counterparts.

Such a hotspot of schizophrenia-associated changes in the upper cortical layers might arise during cortical development. Upper cortical layer principal neurons in the DLPFC start intensive differentiation during the third trimester (*63*). At the same developmental period, GABAergic interneurons that are destined for the upper cortical

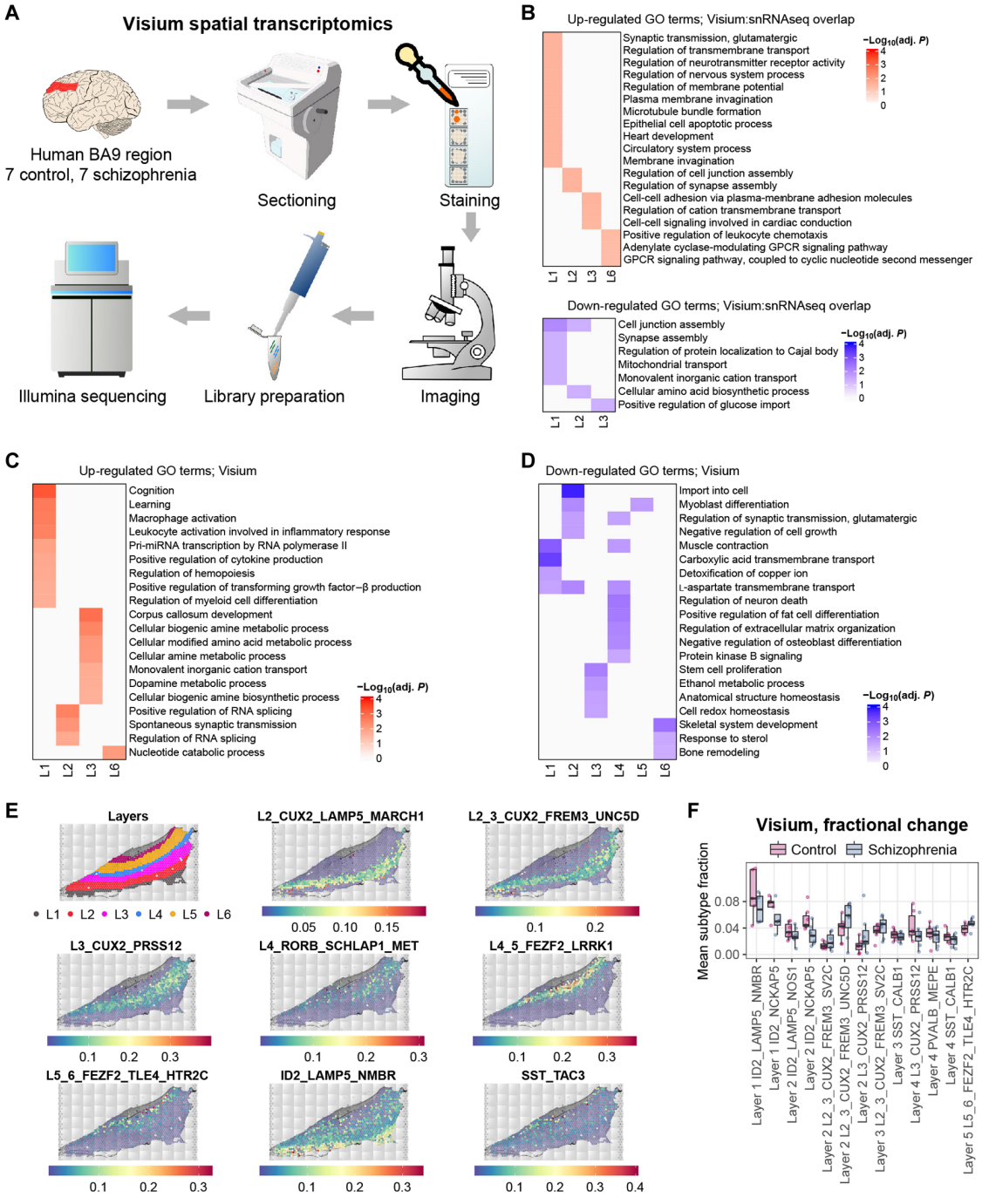

Fig. 7. Spatial transcriptomics analysis identified local transcriptional and compositional perturbations. (**A**) Experimental scheme for spatial transcriptomics. (**B**) Individual GO terms in neuronal subtypes in the DLPFC of patients with schizophrenia that were enriched in up-regulated genes in both snRNA-seq and spatial transcriptomics data. GO term *P* values were Benjamini-Hochberg–corrected. (**C** and **D**) Clusters of GO terms in neuronal subtypes in the DLPFC of patients with schizophrenia that were enriched in up/down-regulated genes in spatial transcriptomics data. Visium spots were aggregated by cortical layer (L1-L6) for DE analysis. *P* values represent Bonferroni-corrected values of 0.05 or lower. (**E**) Spatial location of a selected set of neuronal cell types in Visium data. The location was estimated using Stereoscope cell subtype deconvolution from Visium mini-bulk data. Subtype location largely recapitulates expected spatial distribution demonstrated in Fig. 1E. Fractions of deconvoluted cell subtypes per Visium spot are shown on top of the representative tissue slice. Neuronal subtypes correspond to subtypes identified using snRNA-seq in Fig. 1B. Non-neuronal cell types were predicted using Allen Institute Cell Types Database: RNA-Seq Data Human M1 - 10x Genomics reference dataset (*84*). The detailed location of all subtypes across all samples is demonstrated in fig. S14. (**F**) Changes in neuronal composition in the DLPFC of patients with schizophrenia that were identified in the spatial transcriptomics data. Normality was tested using Shapiro-Wilk test, and equality of variances was tested using Levene's test. As part of the data was not normally distributed, independent two-group Mann-Whitney *U* test was used to test significance of differences for all group pairs. Multiple comparison correction was done using the Benjamini-Hochberg method. Line inside the box represents median, and lower and upper hinges of the box correspond to the first and third quartiles. Upper and lower whiskers correspond to the smallest and the largest values, and not more than 1.5× interquartile range.

Table 1. The summary of major compositional and transcriptomic changes in the DLPFC of schizophrenia patients. For major compositional changes: decrease (↓) or increase (↑) [from low change (one arrow) to high change (three arrows)] of neuronal subtypes; based on compositional data analysis (Fig. 2B and fig. S6C), fraction of nuclei (fig. S6, A and B)—snRNA-seq column, immunohistochemistry (IHC) (Figs. 3 and 4), bulk deconvolution analysis (fig. S6D), and Visium (Fig. 7 and fig. S14). For major transcriptomics changes: from low (+) to high change (+++); based on expression distance (Fig. 2, C and D), pathways (Fig. 5, H and I, and figs. S8 to S12), transcription factor networks (Fig. 6, A and B, and fig. S13)—snRNA-seq column, and Visium (Fig. 7). n.a., not available; n.s., not significant.

Type of measurement	Subtypes	snRNA-seq		IHC	Bulk deconvolution	Visium
		Compositional data analysis	Fraction of nuclei			
Major compositional changes	SST interneurons	↓↓↓	↓↓	n.a.	n.a.	n.s.
	SST_CALB1 (L2-L3)	↓↓↓	↓↓			n.s.
	SST_STK32A (L3-L4)	↓↓	↓↓			n.s.
	SST_NOS1 (L3)	↓↓	↓			n.s.
	PV interneurons	↓	↓	n.s.	n.a.	n.s.
	VIP interneurons	↓	n.s.	↓*	n.a.	n.s.
	L2_3_CUX2_FREM3 principal neurons	↑↑	n.s.	n.a.	↑†	n.s.
	L2_3_CUX2_ FREM3_SV2C	↑↑	n.s.			n.s.
	L2_3_CUX2_ FREM3_UNC5D	↑↑	n.s.			n.s.
	L4_5_FEZF2_LRRK1 principal neurons	↑↑	n.s.	n.a.	↑†	n.s.

Type of measurement	Subtypes	snRNA-seq				Visium
		Expression distance	Pathways	TF networks	Genetics	
Major transcriptomic changes	SST interneurons	++	++	++	+++	n.a.
	SST_CALB1 (L2-L3)	+++	++	+++	++	
	PV interneurons	+++	+++	+++	++	n.a.
	PVALB_CRH (L2-L3)	+++	+++	+++	++	
	PVALB_SST (L2-L3)	+++	+	++	+	
	L2_CUX2_LAMP5 principal neurons	+++	++	+++	+++	+++‡
	L2_CUX2_ LAMP5_PDGFD	+++	+++	+++	+++	+++‡
	L2_CUX2_ LAMP5_MARCH1	+++	+	+++	++	+++‡

*Labeled as CR-positive GABAergic neurons; for correspondence of CR expression (gene *CALB2*) with Vip expression (gene *VIP*), see Fig. 3D. †Analyzed at family level, L2_3_CUX2 and L5_6_FEZF2. ‡Based on layer-wise analysis.

layers arrive and spread (*64*). Human cortical development at late gestation period is characterized by large-scale transcriptomic transition from embryonic to mature neuron transcriptome (*65*), which includes reshaping of the transcriptome involved in neuronal differentiation and maturation (*65*, *66*). Thus, any sort of dysfunction that may arise from genetic variance or environmental perturbation could have long-lasting and severe consequences, which might manifest at the cortical network level. It is important to note that upper cortical layer neurons have a highly protracted synaptic spine overproduction within cortico-cortical circuitries, where final synaptic removal coincides with the appearance of schizophrenia symptoms (*67*). Therefore, our data support the theory that schizophrenia-associated developmental events occur in the DLPFC during late gestation due to the disturbed arrival and integration of GABAergic interneurons into the cortical circuitry and differentiation of principal neurons.

Our work also highlights the possible role of a hitherto less well-characterized interneuron family, the CR^+ neurons, in the etiology of schizophrenia. Our study is the first to demonstrate the "layer 2 low CR cellular phenotype" in schizophrenia. The involvement of this interneuron family in schizophrenia is particularly intriguing,

because there are data showing that this neuron class became the dominant GABAergic population in the primate prefrontal cortex (*42*). In rodents, CR^+ neurons represent 2 to 3% of the total neuronal pool, whereas in the monkey and human prefrontal cortex their proportion can extend to 15% of total neurons. The fact that only 50% of schizophrenia cases manifested this low CR pattern offers the possibility of distinct cellular and molecular phenotypes existing in different types and stages of schizophrenia. High interindividual variability of gene expression found in patients with schizophrenia in our study also confirms the heterogeneity of schizophrenia present at the transcriptomic level.

Upper cortical layer neurons were reported to be the most affected in an snRNA-seq study of another psychiatric disorder: autism spectrum disorder (*68*). Our genetic integration analysis also showed an enrichment of autism spectrum disorder–associated gene expression in DEGs of upper-layer neuronal subtypes, in particular GABAergic interneurons. Thus, the resemblance of the effect of schizophrenia and autism on upper-layer cortical layers may indicate a particular vulnerability of upper-layer neuronal circuits to psychiatric disorders.

Our work also shows that schizophrenia-associated changes do not affect only a selected family of neurons but involve multiple neuronal subtypes, indicating a general network impairment. This widespread impact is manifested by the orchestrated down-regulation of energy metabolism and up-regulation of neurotransmission genes across multiple subtypes of principal neurons and GABAergic interneurons spanning mainly upper cortical layers with involvement of FEZF2 principal neurons from lower layers. Similar changes have been previously noted in association with mental disorders based on genetics and bulk transcriptomics studies (*5*, *65*, *69*). These general impairments during schizophrenia could arise from dysregulation of transcription factor expression affecting many neuronal subtypes, and we identified potential regulons that could contribute to such dysregulation.

Our study also points toward challenges in the current and prospective schizophrenia treatments. We show that instead of a few single neuronal subtypes or genes, schizophrenia-associated changes include a complex circuitry with multiple neuronal subtypes and intracellular signaling networks. Thus, therapies directed at a single specific protein or cell subtype might be ineffective. We also show a number of transcription factors being misexpressed in schizophrenia. Regulons that are associated with these transcription factors could underlie the phenotype in schizophrenia, which could be established during brain development and circuit maturation. Future strategies to identify previously unknown targets for schizophrenia therapy might focus on identifying central hubs in transcriptomic networks across the overarching schizophrenia-associated circuit and designing ways to specifically affect these hubs during circuit maturation.

Throughout our analysis, we observed a prevailing impairment of neuronal subtypes residing in the upper layers of the cortex, which involves subtypes of GABAergic neurons from all four families—PVALB, SST, VIP, and ID2—and L2_3_CUX2 subtypes of principal neurons; additionally, several subtypes of L4_6_FEZF2 principal neurons (most of them—L4_5_FEZF2_LRRK1) showed significant compositional and transcriptomic changes. It is known that upper layers receive information from other cortical and subcortical areas (*70*) and are critical for human cognition (*71*), while lower layer principal neurons are known to transmit information projecting to other regions of the brain. Overall, schizophrenia-associated brain circuits might include a large assembly of neuronal circuitry that sends information into the cortex, where it is received, transformed, and forwarded to other cortical and subcortical regions. Connectivity studies certainly show the central position of the prefrontal cortex within the schizophrenia-associated circuitry, showing impaired connectivity between the prefrontal cortex and, for instance, the amygdala (*72*) and striatum (*73*, *74*). Therefore, the upper-layer neuronal network in the prefrontal cortex might be the central player that underlies impairment of information transfer in schizophrenia. While involvement of both cortical GABAergic and principal neurons in schizophrenia has been known for decades, our work pinpoints specific upper cortical layer GABAergic and principal neuron subpopulations manifesting the most marked transcriptomic changes. The DE reported at subtype-specific resolution provides targets in case of receptor signaling, metabolic, and other pathways for future mechanistic approaches that will aim to dissect the developmental mechanisms of schizophrenia. Last, because current single-cell datasets to study human disorders are relatively small (because of scarcity of good quality material required for snRNA-seq, lack of detailed patient history, high costs, etc.), some of the changes in cell type abundance and transcriptomics may derive from biological covariates, such as medication, comorbidities, lifestyle, and environmental factors. Thus, future studies with larger sets of samples with extensive patient history information that are stratified on the basis of known covariates should be established to provide more definite answers on the impact of each biological covariate on cell type abundance and transcriptomics.

MATERIALS AND METHODS

Summary for software and tools implemented in the study

See Table 2 for the details.

Human subjects

Postmortem human brain tissue was provided by the Netherlands Brain Bank (NBB) Netherlands Institute for Neuroscience, Amsterdam (open access: www.brainbank.nl), the Oxford Brain Bank (OBB), the Human Brain Tissue Bank (HBTB; Semmelweis University, Hungary), and the Newcastle Brain Bank, UK (Newcastle). The experiments were approved by the Ethical Committee in the Capital Region of Denmark, the Committee of Science and Research Ethics of the Ministry of Health, Hungary, and the Regional Committee of Science and Research Ethics of Semmelweis University. Clinical diagnosis of schizophrenia was based on The Diagnostic and Statistical Manual of Mental Disorders (DSM), Third and Fourth Editions. Cases without history of psychiatric disorders were included as controls. All material was collected from donors from whom written informed consent had been obtained by the NBB, OBB, HBTB, or Newcastle for brain autopsy and use of material and clinical information for research purposes. To form the sample set for our study, we aimed to select samples to avoid variability in age, PMI, and other major confounders, which could increase the noise and mask biologically relevant data. The demographic characteristics of the cohort are shown in tables S1, S2, and S6. Sampling was done by assistants of the NBB, OBB, HBTB, and Newcastle supervised by trained neuropathologists. Both paraffin-embedded sections and fresh-frozen tissue blocks were provided from the DLPFC (BA9).

The samples that were used for each type of the analysis are indicated in table S2. Although most samples were used for both snRNA-seq and IHC, few samples were studied only by one of these

Table 2. Summary for software and tools implemented in the study.

Software and tools	Source	Identifier
BD FACSDiva	BD	8.0.1
FCS Express 7 Plus	De Novo Software	v7.04.0014
Cellranger	10x Genomics	v3.1.0
Interop	Illumina	v1.1.10
bcl2fastq	Illumina	2.20.0
pagoda2	https://github.com/kharchenkolab/pagoda2	v0.1.1
Conos	https://github.com/kharchenkolab/conos	v1.2.1, dev
R	www.r-project.org/	3.5.3, 4.0.2
RStudio	https://rstudio.com/	1.2.1335
Zen	Zeiss	2.3
FIJI	https://imagej.net/Fiji	1.52p
Loupe Browser	10x Genomics	v4.1.0
spaceranger	10x Genomics	v1.1.0
Seurat	https://satijalab.org/seurat/	v3.1.4, v3.2.012
DoRothEA	https://github.com/saezlab/dorothea	v1.5
VIPER	https://bioconductor.org/packages/viper/	v1.26.0
CELLEX	https://github.com/perslab/CELLEX	v1.2.1.
CELLECT	https://github.com/perslab/CELLECT	v1.3.0
MuSiC	https://xuranw.github.io/MuSiC	v0.1.1
ggplot2	www.rdocumentation.org/packages/ggplot2/versions/3.3.2	v3.3.2
ggthemes	www.rdocumentation.org/packages/ggthemes/versions/3.5.0	v3.5.0
nlme	www.rdocumentation.org/packages/nlme/versions/3.1-150	v3.1-150
multcomp	www.rdocumentation.org/packages/multcomp/versions/1.4-14	v1.4-14
emmean	https://cran.r-project.org/web/packages/emmeans/index.html	v1.7.3

methods, because of the limited availability of tissue in brain banks or the availability of only fresh-frozen or only formalin-fixed tissue. Some samples had too high PMI to study them for transcriptomics and thus were studied only by histology. All samples for spatial transcriptomics were also analyzed by snRNA-seq.

The schizophrenia and control groups were balanced with respect to multiple other characteristics, including sex, medication, and smoking (fig. S1). Nevertheless, some covariates cannot be completely separated in observational data, for instance, due to the current standards of treatment, and patient lifestyle or medication can potentially influence gene expression in neuronal cell types.

Nucleus isolation

Whenever possible, schizophrenia and control samples were processed in parallel, two samples per experiment. Tissue was removed from −80°C and placed in a 1-ml Dounce homogenizer with 1 ml of chilled homogenization buffer [250 mM sucrose, 25 mM KCl, 5 mM $MgCl_2$, 10 mM tris (pH 8.0), 1 mM dithiothreitol (DTT), 1× protease inhibitor (Roche, 11873580001), ribonuclease (RNase) inhibitor (0.4 U/μl; Takara, 2313B), SUPERase•In (0.2 U/μl; Invitrogen, AM2696), and 0.1% Triton X-100] on ice. Tissue was homogenized with 5 strokes of loose pestle and 15 strokes of tight pestle. Homogenate was filtered through a 40-μm cell strainer and spun down at 1000*g* for 8 min at 4°C. The pellet was gently resuspended in a homogenization buffer with the final volume of 250 μl on ice. Suspension was mixed with 250 μl of 50% iodixanol solution [25 mM KCl, 5 mM $MgCl_2$, 10 mM tris (pH 8.0), 50% iodixanol (60% stock from STEMCELL Technologies, 7820), 1× protease inhibitor (Roche, 11873580001), RNase inhibitor (0.4 U/μl; Takara, 2313B), SUPERase•In (0.2 U/μl; Invitrogen, AM2696), and 1 mM DTT] and overlaid on top of 29% iodixanol solution [25 mM KCl, 5 mM $MgCl_2$, 10 mM tris (pH 8.0), 29% iodixanol, 1× protease inhibitor (Roche, 11873580001), RNase inhibitor (0.4 U/μl; Takara, 2313B), SUPERase•In (0.2 U/μl; Invitrogen, AM2696), and 1 mM DTT] in the ultracentrifuge tube (Beckman Coulter, 343778) on ice. Gradients were spun down in the ultracentrifuge (Beckman Coulter, MAX-XP) using a swing bucket rotor (Beckman Coulter, TLS 55) at 14,000g_{max} for 22 min at 4°C with slow acceleration and deceleration. Following, supernatant was carefully removed, and pellets were resuspended in ice-cold bovine serum albumin (BSA) solution [1× phosphate-buffered saline (PBS) (AM9625, Ambion), 0.5% BSA (VWR, 0332-25G), 1 mM DTT, 2.4 mM $MgCl_2$, and RNase inhibitor (0.2 U/μl; Takara, 2313B)] and incubated on ice for 15 min for blocking. Suspension was split into experimental and fluorescence-activated cell sorting (FACS) control (isotype control, negative control, 7-Aminoactinomycin D (7AAD) only control, and NeuN-only control) samples. Experimental sample and NeuN-only control were stained with antibody against the neuronal marker NeuN (Merck Millipore, MAB3777x, 1 μg/μl) at 1:1890 dilution for 10 min at 4°C protected from light. Isotype control was stained using control antibody (STEMCELL Technologies, 60070AD.1, 0.2 μg/μl) at 1:378 dilution for 10 min at 4°C protected from light. Following, 1 ml of BSA solution was added, and suspensions were mixed and centrifuged for 10 min at 1000*g* at 4°C using a swing bucket rotor. Pellets were resuspended and filtered through 35-μm strainers. Experimental sample, isotype control, and 7AAD-only control were supplemented with 0.75 μl of 7AAD (1 mg/ml) per 0.5 ml of suspension. FACS was done using a BD FACSAria III sorter using a 75-μm nozzle and controlled by BD FACSDiva 8.0.1 software. Compensations were done on the basis of single-color controls. Gates were set on the basis of FACS controls. Nuclei were selected on the basis of FSC-A/SSC-A gate, doublets were removed using FSC-W/FSC-H and SSC-W/SSC-H gates, nuclei were further selected on the basis of 7AAD staining, and neuronal nuclei were sorted on the basis of NeuN

staining. Nuclei were kept at 4°C during FACS and sorted into 5 μl of BSA solution at 4°C. Nuclei were processed directly for 10x library preparation. A complete detailed protocol is available at https://singlecell.ku.dk/protocols/.

Representative FANS plots in fig. S2A were prepared using FCS Express 7 Plus v7.04.0014 (De Novo Software). For confirmation of negligible amount of neuronal nuclei in NeuN$^-$ fraction, see our previous report (*30*).

Samples MB8 and MB8-2 derive from the same patient. Nuclei isolation from separate pieces of cortex and 10x Genomics library preparation were done twice for this patient.

10x library preparation and sequencing

Chromium Single Cell 3′ Reagent Kits v3 (10x Genomics, PN-1000075) were used for library preparation according to a standard protocol. In brief, nuclei were counted under microscope, mixed with reverse transcription mix, and partitioned together with v3 Gel Beads on Chromium Chip B (10x Genomics, PN-1000073) into Gel Beads-in-emulsion (GEMs) using Chromium Controller (10x Genomics, PN-120223). Following reverse transcription, samples were frozen at −20°C. Within a week, samples from several 10x runs were processed together for complementary DNA (cDNA) cleanup and preamplification [12 polymerase chain reaction (PCR) cycles]. After SPRIselect cleanup, cDNA was quantified and frozen at −20°C. In general, the same quantity of cDNA was used during fragmentation, end-repair, and A-tailing for most samples. Following, fragments were cleaned up using SPRIselect reagent and processed through steps of adapter ligation, SPRIselect cleanup, and sample index PCR [using Chromium i7 Sample Indices (10x Genomics, PN-120262) for 11 PCR cycles]. Following, libraries were cleaned up with SPRIselect reagent and quantified using the Qubit HS dsDNA Assay Kit (Thermo Fisher Scientific, Q32854) and Qubit Fluorometer and also using the High Sensitivity DNA Kit (Agilent, 5067-4626) and Agilent 2100 Bioanalyzer. Libraries were pooled according to the expected amount of nuclei per sample; pool was quantified and sequenced using either 100 or 200 cycles of NovaSeq 6000 S2 (Illumina, 20012861 and 20012862) runs on Illumina NovaSeq 6000 System (Illumina 20012850) controlled by NovaSeq Control Software. Libraries were sequenced using 28 cycles for read 1, 8 cycles for i7 index, and 94 cycles for read 2. On average, there were 54,230 reads and 4413 genes per nucleus.

Single-nucleus sequencing data analysis

Quality of sequencing data was checked using Illumina's interop v1.1.10 tool. Primary data analysis was performed using cellranger v3.1.0 (10x Genomics). Release 97 of human genome from Ensembl was used:

http://ftp.ensembl.org/pub/release-97/fasta/homo_sapiens/dna/Homo_sapiens.GRCh38.dna.primary_assembly.fa.gz

http://ftp.ensembl.org/pub/release-97/gtf/homo_sapiens/Homo_sapiens.GRCh38.97.gtf.gz

GTF file was modified to create pre-mRNA reference ("transcript" was renamed to "exon" and retained in the final gtf: awk 'BEGIN{FS = "\t"; OFS = "\t"} $3 == "transcript"{$3 = "exon"; print}' Homo_sapiens.GRCh38.97.gtf > Homo_sapiens.GRCh38.97.PREmRNA.gtf). Then, the reference genome was created using cellranger mkref. Illumina .bcl files were demultiplexed using cellranger mkfastq pipeline; reads were mapped against reference genome, and UMIs were counted using cellranger count pipeline. Filtered feature barcode matrices were used for further secondary analysis.

Secondary analysis was performed using pagoda2 (https://github.com/kharchenkolab/pagoda2) and Conos (https://github.com/kharchenkolab/conos). To eliminate potential doublets, scrublet scores were determined for each dataset, and only cells with the score below 0.3 were considered for downstream analysis. Each dataset was normalized using pagoda2 with default parameters, requiring at least 500 molecules per cell. Different samples were then aligned using Conos with default parameter settings [principal components analysis (PCA) space with 30 components, angular distance, mNN matching, $k = 15$, k.self = 5], and UMAP embedding was estimated using default parameter settings.

Normality of the distribution of fractions of nuclei derived from different neuronal subtypes (Fig. 2B and fig. S6, A and B) was tested using Shapiro-Wilk test (shapiro.test), and equality of variances was tested using Levene's test (leveneTest). As part of the data was not normally distributed, independent two-group Mann-Whitney *U* test (wilcox.test) was used to test significance of differences for all group pairs. Multiple comparison correction was done using the Benjamini-Hochberg method.

Gene expression plots (Figs. 5B and 7F and fig. S12G) were based on normalized pseudo-bulk gene expression levels. UMI counts were summed up separately for each gene across all cells derived from a specific subtype-sample combination. Subtype-sample combinations with less than 10 cells were filtered out. Pseudo-bulk counts were then normalized: divided by the sum of all counts across all genes in any particular subtype-sample combination and multiplied by 10^6. *P* values were estimated using differential gene expression Wald test in DESeq2. Multiple comparison correction was done using the Benjamini-Hochberg method.

Compositional data analysis

We performed compositional analyses as described elsewhere (*34*, *35*, *75*) using the Cacoa function estimateCellLoadings() (coda.test = "significance"). In short, isometric log-ratio transformations were applied to cell type fractions followed by canonical discriminant analyses using the candisc package to obtain weighted contrasts between cell types in schizophrenia and control samples. Random cell subsamplings were applied to evaluate robustness and statistical significance of the separating coefficients. In total, 1000 subsamplings were performed each time evaluating 1000 randomly sampled cells from both groups to evaluate test robustness. The separating coefficients are plotted. Multiple comparison correction was done using the Benjamini-Hochberg method.

Estimation of differential cell density

Differential cell density was performed through the estimateCellDensity() function from Cacoa (*75*). To estimate differential cell density between sample groups, we first compute kernel density in joint embedding space for each sample using the ks R package (bin = 400). Then, quantile normalization was used to normalize the density matrix across samples. The average density of each sample group was shown in Fig. 2A. To impute the differential cell density between sample groups, we performed *t* test between sample groups in each girded bin. To avoid noise from the background, we filtered bins with at least one cell and the z score is shown as heatmap. Sample labels were randomly permuted 200 times to evaluate test robustness. We have implemented a correction procedure for the density tests as described in (*76*), which is based on the distribution of the maximal statistic under permutations of condition labels.

Validation of compositional changes using deconvolution on bulk samples

Allen Institute dataset (H18.30.001 and H18.30.002 samples) and samples mapped to Allen Institute reference genome (MB14, MB15, and MB17) were merged with mergeCountMatrices function (Conos v1.4.2) and processed through Pagoda2 v1.0.4 log scale normalization, variance adjustment (gam.k = 10), and PCA reduction (nPcs = 50, n.odgenes = 3000). DEGs were obtained by applying getDifferentialGenes function "one vs. all" for families of excitatory neurons (L2_3_CUX2, L4_6_FEZF2, L4_RORB, and L5_6_THEMIS). In addition, DEGs were filtered to be specific for one cell type only. Normalized counts, the list of differential genes, and the bulk DLPFC dataset (CommonMind: 501 control individuals and 353 with schizophrenia) (*24*, *36*) were submitted to MuSiC v0.1.1 (*77*) deconvolution pipeline - music_prop, music_basis, music_prop.cluster functions using default parameters. We used only bulk counts of DEGs for cell type proportion calculation. Proportions for L2_3_CUX2, L4_6_FEZF2, L4_RORB, and L5_6_THEMIS families of excitatory neurons in bulk DLPFC dataset were calculated on the basis of specific DEGs calculated with Conos and Pagoda2 using MB14, MB15, and MB17 samples only, as described for the merged set. Independent two-group Mann-Whitney *U* test with multiple comparison Benjamini-Hochberg adjustment was used to determine significant changes in cell type proportions between control and schizophrenia.

Expression distance analysis

Expression differences between matching subpopulations were determined by first estimating "mini-bulk" (or meta-cell) RNA-seq measurements for each subpopulation in each sample using the estimateExpressionShiftMagnitudes() function from Cacoa. Briefly, in each dataset, the molecules from all cells belonging to a given subpopulation were summed for each gene (i.e., forgetting cellular barcodes). The resulting high-coverage RNA-seq vectors were normalized by total counts and log-transformed. Then, the distances were calculated using Pearson's linear correlation on these vectors (dist = "cor"). To obtain normalized distance estimates d_n, the expression distances of sample pairs between the conditions (control and schizophrenia) were normalized by subtracting the median expression distance across all sample pairs within the control condition. Last, to adjust for other possible random effects and to estimate statistical significance of the results, we performed 2500 random permutations of the condition labels for samples within each cell type and estimated the null distribution of d_n. Median of this distribution was subtracted from the distances d_n to obtain final values (Fig. 2, C and D). *P* values were estimated as proportion of permutations, resulting in distances of the same or greater magnitude as d_n and were adjusted for multiple comparisons using the Benjamini-Hochberg correction.

Overall, expression distances between samples were determined as a normalized weighted sum of correlation distances across all cell subpopulations contained in both samples, with the weight equal to the subpopulation proportion (measured as a minimal proportion that the given cell subpopulation represents among the two samples being compared). Expression distances between samples are projected to two-dimensional (2D) space using multidimensional scaling (Fig. 2F). To illustrate interindividual expression distance within each sample group, intersample expression distance is shown as a boxplot (Fig. 2E).

To determine expression distance along a consensus direction (fig. S7, B and C), we used the estimateCommonExpressionShiftMagnitudes() function from Cacoa. For each cell type, a consensus expression shift between control and schizophrenia conditions was determined by calculating a trimmed mean $\log_2$ fold expression change for each gene. The resulting shift vector was normalized by its Frobenius norm to obtain the consensus shift vector *v*. For each pair of samples, the normalized distance was determined as a dot product between the $\log_2$ fold expression change vector for a given pair and the normalized consensus shift vector *v*. As in the previous case, null distribution of these distances was estimated using permutation of condition labels and was used to obtain the final magnitudes and *P* values.

Differentially expressed genes

DE was performed on normalized pseudobulk gene counts using the Wald test in DESeq2 (*78*) through the estimatePerCellTypeDE() function in (*75*). In short, gene counts per cell type were collapsed per sample to create pseudobulk gene counts. Benchmarking has proved this to be an effective approach for DEG discovery in single-cell studies, and DESeq2 was one of the best-performing methods (*79*). Then, DEGs are determined using a grouping factor as a model for expression (schizophrenia versus control). A fixed number of 80 cells was used for DE estimation as well as group randomization to evaluate robustness of our results. DE results were used as input for GO estimations. Multiple comparison correction of DEGs was done using the Benjamini-Hochberg method.

Gene ontology

GO enrichment was investigated using the clusterProfiler (*80*) package. Enrichment was evaluated per cell type for GO biological pathways (BP) categories on sets of top 500 up- and down-regulated genes separately based on *z* score. To calculate GO terms, we used as background only genes expressed within a cell type. Resulting BP categories were filtered by *P* value <0.001 and corrected for multiple comparison as every GO term * every cell type using the Bonferroni method. GO terms with an adjusted *P* value <0.05 were clustered into 20 clusters based on the similarity of the genes involved in the categories using binary distance measures. The clusters were named on the basis of the most significantly enriched category.

Estimation of transcription factor networks based on gene expression from snRNA-seq data

Transcription factor enrichment was calculated using the VIPER (*48*) and DoRothEA packages (*47*). DoRothEA regulons A, B, and C were selected by their confidence score and were used together with DEGs as input for VIPER. The estimated enrichment score was calculated on the basis of the z score of the DEGs and was normalized for the purpose of hierarchical clustering. Hierarchical clustering of selected transcription factors was done using the ComplexHeatmap package (method = "ward.D2").

Integration of snRNA-seq and genetics data

To integrate with datasets of genes previously associated with schizophrenia, from the DisGeNET database (*60*), and autism spectrum disorder, from the SFARI database, we performed hypergeometric testing to identify significant overlaps between DEGs in our dataset with genes from each of the abovementioned datasets. We took the 500 most DEGs per cell subtype as the sample input, and we used all expressed genes in our dataset as the background. The resulting Bonferroni-corrected *P* values are shown.

To integrate our snRNA-seq data with the largest schizophrenia GWAS dataset (*61*), we used CELLECT (*81*) and GWAS data on 40,675 schizophrenia patients and 64,643 controls (*61*). First, we computed cell type expression specificity profiles using CELLEX. Then, we munged the GWAS summary statistics according to the CELLECT tutorial. Last, we identified disease-relevant cell types using the linkage disequilibrium score regression algorithm incorporated in CELLECT, using a 100-kb genomic window. The resulting Bonferroni-corrected *P* values are shown.

Assessment of potential contribution of antipsychotic drugs on gene expression in schizophrenia samples

Two approaches have been implemented—comparison to antipsychotic signatures from the DLPFC of rhesus macaque treated with haloperidol or clozapine and comparison to antipsychotic signatures from the DLPFC of human schizophrenia patients that were treated with antipsychotics (compared to those that were not treated).

DE analysis of placebo-, haloperidol-, and clozapine-treated rhesus macaque DLPFC bulk samples (CommonMind: clozapine, 9; haloperidol, 17; placebo, 8) (*24*, *36*) was done in edgeR v3.32.1 (glmFit and glmLRT). Raw counts were trimmed mean of M values (TMM) normalized following trended and tagwise dispersions estimation. DEGs were obtained through glmFit and glmLRT functions ($P < 0.05$). Gene list was reduced to one-to-one gene orthologs with biomaRt v2.46.3.

In addition, a list of DEGs was obtained from a human DLPFC antipsychotic dataset (*44*). DEGs were selected the same way as for the rhesus macaque dataset ($P < 0.05$). Overlaps of rhesus macaque DEGs and the human antipsychotic DEGs with DEGs from our snRNA-seq dataset were tested by hypergeometric test, and *P* values were adjusted with Benjamini-Hochberg correction.

Estimation of cortical layer positions of neural cell subtypes

Locations of neural cell subtypes were estimated from the Allen Institute human motor cortex (M1C), temporal cortex (MTG), and anterior cingulate cortex (CgG) datasets (*32*, *33*): https://transcriptomic-viewer-downloads.s3-us-west-2.amazonaws.com/human/transcriptome.zip and https://transcriptomic-viewer-downloads.s3-us-west-2.amazonaws.com/human/sample-annotations.zip.

To minimize differences between our (KU) and Allen Institute single-nucleus datasets, we remapped KU samples against Allen Institute genome reference: RefSeq Genomic FASTA (www.ncbi.nlm.nih.gov/assembly/GCF_000001405.28/) and GTF (http://celltypes.brain-map.org/api/v2/well_known_file_download/502175284).

Allen Institute GTF file was modified using gffread (*82*) as follows: gffread rsem_GRCh38.p2.gtf -T -v -F --keep-genes --keep-exon-attrs -o rsem_GRCh38.p2_2.gtf.

Then, gene_symbol was renamed into gene_name: sed 's/gene_symbol/gene_name/g' rsem_GRCh38.p2_2.gtf > rsem_GRCh38.p2_3.GTF.

pre-mRNA GTF was created as follows: awk 'BEGIN{FS = "\t"; OFS = "\t"} $3 == "transcript" {$3 = "exon"; print}' rsem_GRCh38.p2_3.GTF > rsem_GRCh38.p2_3_premRNA.GTF.

Following, an Allen Institute genome reference was created using cellranger mkref. KU MB14, MB15, and MB17 sample reads were remapped against the Allen Institute reference genome, and UMIs were counted using the cellranger count pipeline. Pagoda2 v0.1.1 run under R version 3.5.3 in RStudio version 1.2.1335 was used to create pagoda objects from feature barcode matrices using basicP2proc with n.odgenes = 3000, min.cells.per.gene = 0, min.transcripts.per.cell = 0 parameters. Conos v1.2.1 was used to create conos objects with Conos$new. KU single-nucleus and Allen Institute datasets (either MTG, M1C, or CgG) were integrated using con$buildGraph with parameters $k = 30$, k.self = 5, space = "PCA," ncomps = 30, n.odgenes = 3000, matching.method = "mNN," metric = "angular"; parameters alignment.strength and same.factor.downweight were individually tweaked to optimize integration between datasets.

Following, high- or medium-resolution (not shown) subtype annotations were transferred from KU single-nucleus to Allen Institute datasets using conos$propagateLabels. Subtype labels were given on the basis of the highest probability of a nucleus to belong to a certain subtype. Then, cortical layer positions of Allen Institute nuclei (derived from microdissections of cortical layers before FANS of nuclei) were used for plotting cortical positions of KU neural cell subtypes (Fig. 1). Location estimation from all three regions (M1C, MTG, and CgG) produced similar results, with MTG estimates being demonstrated on Fig. 1E. Because layer annotation of cell type positions is based on manual dissection of cortical layers before nucleus isolation, small discrepancies between predicted and actual positions of cell types are expected, such as the presence of excitatory neurons in layer 1.

Human cortex slice preparation for Visium analysis

Tissue slices were prepared according to the standard Visium tissue preparation guide (10x Genomics, CG000240). Slices were mounted on Visium Gene Expression Slides (10x Genomics, 2000233) from the Visium Spatial Gene Expression Slide Kit (10x Genomics, PN-1000185), two from patients with schizophrenia, and two from controls on the same slide.

Tissue staining, imaging, and Visium library preparation

Tissue slices were processed according to the standard Visium Methanol Fixation and H&E Staining guide (10x Genomics, CG000160). In brief, slices were fixed in methanol and stained with hematoxylin, followed by bluing and eosin staining. Slices were covered with mounting medium [85% glycerol, RNase inhibitor (4.4 U/μl; Takara, 2313B), and 1 mM DTT] and coverslips before imaging. Slides were imaged using an Axio Observer.Z1/7 confocal microscope (Zeiss) controlled by Zen 2.3 software. Images were preprocessed using FIJI 1.52p (*83*).

Straight after imaging, coverslips were removed using 3× SSC buffer and samples were directly processed according to the standard Visium Spatial Gene Expression protocol (10x Genomics, CG000239) using the Visium Spatial Gene Expression Slide & Reagent Kit (10x Genomics, PN-1000184). Tissue was permeabilized during 12 min, and mRNA was reverse-transcribed, followed by second-strand synthesis and denaturation. cDNA was quantified using KAPA SYBR FAST qPCR Master Mix (Roche, KK4600) on LightCycler 480 Real-Time PCR System (Roche) to determine an optimal amount of PCR cycles required for cDNA preamplification. Seventeen to 19 cycles were used for cDNA preamplification, followed by cDNA cleanup with SPRIselect reagent (B23318, Beckman Coulter) and cDNA quantification. Same amount of cDNA was used for fragmentation, end repair, and A-tailing step. Following, SPRIselect cleanup, adaptor ligation, another SPRIselect cleanup, and sample index PCR [13 cycles, using Dual Index Kit TT (10x Genomics, 1000215)] steps were performed. Libraries were cleaned up using

SPRIselect reagent and quantified using the High Sensitivity DNA Kit run on Agilent 2100 Bioanalyzer and also KAPA Illumina library quantification kit (Roche, 7960140001) run on LightCycler 480. Tissue-covered spots were quantified using Loupe Browser v4.1.0 (10x Genomics), and libraries were pooled according to their concentration and spot occupation on slides. Library pool was quantified on Bioanalyzer and with quantitative PCR and sequenced using the NextSeq 500/550 High Output Kit v2.5 (Illumina, 20024907) on Illumina NextSeq 500 using these parameters: read 1, 28 cycles; i7 index, 10 cycles; i5 index, 10 cycles; read 2, 90 cycles.

Visium spatial transcriptomics data analysis

Primary data analysis was performed using spaceranger v1.1.0 (10x Genomics). Visium metadata are listed in table S6. Two reference genomes were used. Release 97 of human genome from Ensembl was used to generate feature barcode matrices for differential gene expression and GO analyses: http://ftp.ensembl.org/pub/release-97/fasta/homo_sapiens/dna/Homo_sapiens.GRCh38.dna.primary_assembly.fa.gz and http://ftp.ensembl.org/pub/release-97/gtf/homo_sapiens/Homo_sapiens.GRCh38.97.gtf.gz.

While the Allen Institute reference was used to prepare feature barcode matrices for Stereoscope (*83*) cell type deconvolution: RefSeq Genomic FASTA (www.ncbi.nlm.nih.gov/assembly/GCF_000001405.28/) and GTF file (http://celltypes.brain-map.org/api/v2/well_known_file_download/502175284).

Allen Institute GTF file was modified to rename gene_symbol into gene_name: sed 's/gene_symbol/gene_name/g' rsem_GRCh38.p2.gtf > rsem_GRCh38.p2_GENE_NAME.GTF.

Following, reference genomes were created using spaceranger mkref. Illumina .bcl files were demultiplexed using spaceranger mkfastq pipeline; reads were mapped against reference genomes, and UMIs were counted using spaceranger count pipeline. For samples where tissue section covered fiducial frame on Visium slide, manual fiducial alignment and tissue outlining were performed in Loupe Browser; .json file with coordinates was then submitted during spaceranger run with the "-- loupe-alignment=" parameter. Filtered feature barcode matrices were used for further analysis. In addition, low-quality tissue areas were excluded manually and cortical layers were annotated by an experienced histologist using Loupe Browser v4.1.0 (10x Genomics). White matter was excluded from analysis based on manual cortical layer annotation.

To investigate cell type composition of the spatial transcriptomic samples, we performed deconvolution using Stereoscope. Because the 10x snRNA-seq samples, produced for this study, were depleted from non-neural cells during FACS, we added non-neural cells from Allen Institute Cell Types Database: RNA-Seq Data Human M1 - 10x Genomics (*84*) to our neuronal nuclei: https://idk-etl-prod-download-bucket.s3.amazonaws.com/aibs_human_m1_10x/matrix.csv and https://idk-etl-prod-download-bucket.s3.amazonaws.com/aibs_human_m1_10x/metadata.csv.

Non-neural nuclei were selected on the basis of class_label "Non-neural" in the metadata. Medium-resolution annotation of Allen Institute non-neural nuclei was derived from subclass_label in the metadata, and high-resolution annotation was derived from cell_type_alias_label in the metadata.

We used Seurat v3.1.4 on the MB11 spatial sample to find 3000 highly variable genes, which were later used for the deconvolution. For the deconvolution, we applied Stereoscope using the merged single-cell RNA-seq (scRNA-seq) count matrix to all spatial samples for a different resolution of annotation. For medium resolution, we used 10,000 epochs ("-sce" parameter) and a batch size of 1000 ("-scb") for fitting scRNA-seq data and 20,000 epochs ("-ste") with a batch size of 1000 ("-stb") for fitting spatial data. For high resolution, we used sce = 20000, scb = 1000, ste = 30000, and stb = 1000.

Fractions of deconvoluted cell subtypes per Visium spot were plotted on top of histological images (Fig. 7E) using Seurat v3.2.0 (*85*) run in R. Seurat objects were created using Load10X_Spatial. Manual layer annotation metadata were added to the objects; Stereoscope deconvolution predictions were added to the Seurat objects using CreateAssayObject. Plotting was performed using SpatialPlot, and high-resolution subtypes are shown for the MB11 sample.

Stereoscope predicted fractions of subtypes were averaged per sample per layer per subtype (Fig. 7). Normality of distribution was tested using Shapiro-Wilk test (shapiro.test), and equality of variances was tested using Levene's test (leveneTest). As part of the data was not normally distributed, independent two-group Mann-Whitney *U* test (wilcox.test) was used to test significance of differences for all group pairs. Multiple comparison correction was done using the Benjamini-Hochberg method.

DEGs were estimated using esimatePerCellTypeDE function from Cacoa repository. Then, GO terms were estimated for each layer using 500 genes with the highest/lowest *z* score for up- or down-regulated GOs correspondingly using the clusterProfiler package (*80*). *P* values from DEGs were corrected for multiple comparison using the Benjamini-Hochberg method. GO terms were filtered and corrected for multiple comparison as described in the "Gene ontology" section. To group GO terms that were enriched on the basis of the same genes, we clustered them using Jaccard similarity of the gene sets. For that, pairwise Jaccard distances were estimated on the sets of enriched genes for all GO terms for each layer separately with adjusted *P* values below 0.05. Then, hierarchical clustering was performed on these distances (hclust function with method = "ward.D2"), and the hierarchy was trimmed to 20 clusters. The *P* value of the resulting cluster for a layer was estimated as minimum across all *P* values of the cluster's GO terms. The name of a cluster was set to the name of its term with the lowest geometric mean of *P* values across all layers. To compare results of GO analysis on spatial data to the GO terms discovered on snRNA-seq data, we used only spatial GO that were significantly enriched in snRNA-seq data, adjusted *P* values only on those with a *P* value of <0.05 using the Benjamini-Hochberg correction (which allowed to increase power of the test), and visualized the filtered spatial GO terms with adjusted *P* values below 0.05.

Immunohistochemistry

Consecutive paraffin-embedded brain sections were stained for the five antigens investigated and for Nissl. One section per individual was used per immunostaining (table S5). IHC analysis was done as described in earlier studies (*86*). Briefly, the sections were dewaxed through a graded alcohol series and treated with 3% H_2O_2 solution (in PBS, pH 7.4) for 30 min. Antigen retrieval was applied by autoclaving the slides in citrate buffer (0.01 M, pH 6.0) at 121°C for 10 min. The following primary antibodies were used: anti-CR (rabbit, 1:300, Chemicon, AB5054), anti-NPY (rabbit, 1:250, Abcam, ab30914), anti-CB (mouse, 1:300, Swant, D28k-300), anti-PV (rabbit, 1:500, Abcam, ab11427), and anti-SMI31.1 (mouse, 1:500, BioLegend, 837801) in tris-buffered saline/Triton TMX-100 (pH 7.4)

for 1 hour (100 µl per section). Sections were then incubated with horseradish peroxidase–linked secondary antibody from the Envision Kit (Dako, K-5007) for 1 hour (100 µl per section), and labeling was visualized by DAB from the same Envision Kit applied for 90 s (100 µl per section). During incubation with primary and secondary antibodies, slides were put into Sequenza System coverplates and rack (Thermo Fisher Scientific, 72110017 and 73310017). Two rinses with tris-buffered saline/Triton TMX-100 (pH 7.4) were applied between the above-described steps of IHC (1000 µl each). Hematoxylin nuclear counterstain was applied for 20 s. Sections were dehydrated through a graded alcohol series and coverslipped with DePeX. No labeling was observed when primary antibodies were omitted from the protocol.

Image analysis and quantification

Sections were digitized using a slidescanner (3D Histech) at ×40 magnification. The regions of interest (2 mm × 1 mm columns with all cortical layers present) were outlined using the ImageScope software (Aperio, v11.2.0.780). Designation of cortical layers (BA9) was outlined on the basis of Nissl and SMI31.1 stainings in good agreement with (*87*). Cross-sectional areas analyzed in this study are shown in table S5. The longest diameters of immunopositive cell bodies in the region of interests were manually measured as described in (*86*). Three investigators (V.F., L.R., and E.F.) measured cell diameters on separate sections, and all were blinded to the diagnoses of the subjects through random coding of the subject identifiers. Neuronal cell bodies with a diameter of >4 µm and a width of >2 µm were included in further statistical analysis. Their work was supervised by I.A. checking the annotations. At this stage, minimal (<1%) false positives were detected and less than 5% were false negative. These were corrected by I.A.

Single-molecule fluorescence in situ hybridization

Sections from schizophrenia and control cases were processed for simultaneous detection of target mRNAs (CHRFAM7A, CRH, and VIP) in combination with CR IHC as previously described (*88*, *89*). Paraffin-embedded sections were first deparaffinized and treated with 3% H_2O_2 for 10 min and rinsed in 0.01 M PBS (pH 7.4). Sections were then processed for fluorescence in situ hybridization (RNAscope) using the RNAscope Multiplex Fluorescent Kit V2 (Advanced Cell Diagnostics Inc., Newark, CA, USA; catalog no. 323110) according to the manufacturer's protocol. Briefly, sections were treated with 100% ethanol, incubated in antigen retrieval buffer maintained at a boiling temperature for 10 min, rinsed in PBS, and immediately treated with Protease Plus for 30 min at 40°C. RNAscope Probe – Hs (homo sapiens)-CHRFAM7A-C1 (catalog no. 833991) or CRH-C1 (catalog no. 475211) for detection of target mRNAs and RNAscope Probe Hs-VIP-C2 (catalog no. 452751-C2) for the detection of VIP mRNA were hybridized for 2 hours at 40°C. After hybridization, sections were processed to amplification of target probes and then visualized using the Tyramide Signal Amplification (PerkinElmer, Waltham, MA, USA), fluorescein for CHRFAM7A or CRH mRNA, and Cy3 for VIP mRNA. Following the RNAscope assay, sections were rinsed in PBS and processed for IHC detection of CR. Sections were incubated for 1 hour at room temperature in 3% normal donkey serum (NDS; Vector Laboratories Inc., Burlingame, CA, USA) and overnight at 4°C in the rabbit polyclonal antibody directed against CR (1:300, Millipore, Burlington, MA, USA; AB5054) diluted in PBS containing 0.3% Triton X-100 and 1% NDS. After three washes in PBS, the sections were incubated for 2 hours in Alexa Fluor 647–conjugated donkey anti-rabbit (1:2000; Thermo Fisher Scientific), three times washed in PBS, and mounted by Vectashield (Vector Laboratories Inc., Burlingame, CA, USA).

Statistical analysis of IHC and smFISH data

Results are presented as means ± SD. Density values per case are listed in table S5G. Student's *t* test (unpaired, two-tailed) was used to assess whether the means of cortical width and neuronal diameters of CR- and PV-expressing cells between the two diagnostic groups were significantly different (table S5C). A rigorous $\alpha = 0.01$ was used when reporting statistically significant differences between diagnostic groups. Significance level for normality tests (Shapiro-Wilk test) and correlation tests (Pearson's, applied in case of normal distribution; Spearman's, applied when data did not follow normal distribution) was set to the conventional 5% ($\alpha = 0.05$). The statistical analyses of IHC and smFISH (RNAscope) density data were carried out in R environment. We used the "ggplot2" and "ggthemes" packages for descriptive analysis, and "nlme," "multcomp," and "emmeans" packages for statistical analysis (see links and version in the table "Summary for software and tools implemented in the study"). To incorporate the unique effect of each donor on which multiple measurements were taken, we applied linear mixed models with random effect using the "lme" function of "nlme" package (*90*). Cell types were investigated in separate models. Cell densities were set as dependent variables. Identifiers of individual samples were included as random effect. Layer-wise localization (cortical layers 1 to 6) was set as a six-level within-subject factor, while diagnosis was set as a two-level between-subject factor (schizophrenia or control).

PMI, age, and gender were included as potential confounder variables. Initially, "full" models were constructed including diagnosis, PMI, age, gender, and their interactions with the layer factor. This revealed which variables have significant effects on the dependent variable. Nonsignificant interactions and variables were dropped to achieve the "final" model (table S5F). *P* values were not corrected during model construction. Multiple comparison tests were applied to the final models using the "lsmeans" function to directly compare all layers with each other across the diagnostic groups. *P* values were corrected for multiple testing with the Bonferroni method. Because this approach results in numerous comparison pairs, we only reported the *P* values of comparison pairs relevant to our study (namely, control versus schizophrenia comparisons in layers 1, 2, 3, 4, 5, and 6; table S5F).

SUPPLEMENTARY MATERIALS

Supplementary material for this article is available at https://science.org/doi/10.1126/sciadv.abn8367

View/request a protocol for this paper from Bio-protocol.

REFERENCES AND NOTES

1. GBD 2017 Disease and Injury Incidence and Prevalence Collaborators, Global, regional, and national incidence, prevalence, and years lived with disability for 354 Diseases and Injuries for 195 countries and territories, 1990–2017: A systematic analysis for the Global Burden of Disease Study 2017. *Lancet* **392**, 1789–1858 (2018).
2. M. J. Millan, A. Andrieux, G. Bartzokis, K. Cadenhead, P. Dazzan, P. Fusar-Poli, J. Gallinat, J. Giedd, D. R. Grayson, M. Heinrichs, R. Kahn, M. O. Krebs, M. Leboyer, D. Lewis, O. Marin, P. Marin, A. Meyer-Lindenberg, P. McGorry, P. McGuire, M. J. Owen, P. Patterson, A. Sawa, M. Spedding, P. Uhlhaas, F. Vaccarino, C. Wahlestedt, D. Weinberger, Altering the course of schizophrenia: Progress and perspectives. *Nat. Rev. Drug Discov.* **15**, 485–515 (2016).

3. M. J. Owen, A. Sawa, P. B. Mortensen, Schizophrenia. *Lancet* **388**, 86–97 (2016).
4. D. A. Lewis, T. Hashimoto, D. W. Volk, Cortical inhibitory neurons and schizophrenia. *Nat. Rev. Neurosci.* **6**, 312–324 (2005).
5. N. G. Skene, J. Bryois, T. E. Bakken, G. Breen, J. J. Crowley, H. A. Gaspar, P. Giusti-Rodriguez, R. D. Hodge, J. A. Miller, A. B. Muñoz-Manchado, M. C. O'Donovan, M. J. Owen, A. F. Pardiñas, J. Ryge, J. T. R. Walters, S. Linnarsson, E. S. Lein; Major Depressive Disorder Working Group of the Psychiatric Genomics Consortium, P. F. Sullivan, J. Hjerling-Leffler, Genetic identification of brain cell types underlying schizophrenia. *Nat. Genet.* **50**, 825–833 (2018).
6. N. A. Vasistha, K. Khodosevich, The impact of (ab)normal maternal environment on cortical development. *Prog. Neurobiol.* **202**, 102054 (2021).
7. A. Mukherjee, F. Carvalho, S. Eliez, P. Caroni, Long-lasting rescue of network and cognitive dysfunction in a genetic schizophrenia model. *Cell* **178**, 1387–1402.e14 (2019).
8. J. P. Hamm, D. S. Peterka, J. A. Gogos, R. Yuste, Altered cortical ensembles in mouse models of Schizophrenia. *Neuron* **94**, 153–167.e8 (2017).
9. N. A. Vasistha, M. Pardo-Navarro, J. Gasthaus, D. Weijers, M. K. Müller, D. García-González, S. Malwade, I. Korshunova, U. Pfisterer, J. von Engelhardt, K. S. Hougaard, K. Khodosevich, Maternal inflammation has a profound effect on cortical interneuron development in a stage and subtype-specific manner. *Mol. Psychiatry* **25**, 2313–2329 (2020).
10. P. Steullet, J. H. Cabungcal, J. Coyle, M. Didriksen, K. Gill, A. A. Grace, T. K. Hensch, A. S. LaMantia, L. Lindemann, T. M. Maynard, U. Meyer, H. Morishita, P. O'Donnell, M. Puhl, M. Cuenod, K. Q. Do, Oxidative stress-driven parvalbumin interneuron impairment as a common mechanism in models of schizophrenia. *Mol. Psychiatry* **22**, 936–943 (2017).
11. D. Dwir, B. Giangreco, L. Xin, L. Tenenbaum, J. H. Cabungcal, P. Steullet, A. Goupil, M. Cleusix, R. Jenni, P. S. Baumann, P. Klauser, P. Conus, R. Tirouvanziam, M. Cuenod, K. Q. Do, MMP9/RAGE pathway overactivation mediates redox dysregulation and neuroinflammation, leading to inhibitory/excitatory imbalance: A reverse translation study in schizophrenia patients. *Mol. Psychiatry* **25**, 2889–2904 (2019).
12. J. P. Hamm, Y. Shymkiv, J. Mukai, J. A. Gogos, R. Yuste, Aberrant cortical ensembles and schizophrenia-like sensory phenotypes in Setd1a+/− Mice. *Biol. Psychiatry* **88**, 215–223 (2020).
13. K. K. Cho, R. Hoch, A. T. Lee, T. Patel, J. L. Rubenstein, V. S. Sohal, Gamma rhythms link prefrontal interneuron dysfunction with cognitive inflexibility in Dlx5/6(+/−) mice. *Neuron* **85**, 1332–1343 (2015).
14. J. P. Hamm, R. Yuste, Somatostatin interneurons control a key component of mismatch negativity in mouse visual cortex. *Cell Rep.* **16**, 597–604 (2016).
15. A. B. Van Derveer, G. Bastos, A. D. Ferrell, C. G. Gallimore, M. L. Greene, J. T. Holmes, V. Kubricka, J. M. Ross, J. P. Hamm, A role for somatostatin-positive interneurons in neuro-oscillatory and information processing deficits in schizophrenia. *Schizophr. Bull.* **47**, 1385–1398 (2021).
16. S. Malwade, J. Gasthaus, C. Bellardita, M. Andelic, B. Moric, I. Korshunova, O. Kiehn, N. A. Vasistha, K. Khodosevich, Identification of vulnerable interneuron subtypes in 15q13.3 microdeletion syndrome using single-cell transcriptomics. *Biol. Psychiatry* **91**, 727–739 (2022).
17. J. R. Glausier, K. N. Fish, D. A. Lewis, Altered parvalbumin basket cell inputs in the dorsolateral prefrontal cortex of schizophrenia subjects. *Mol. Psychiatry* **19**, 30–36 (2014).
18. G. P. Reynolds, C. L. Beasley, GABAergic neuronal subtypes in the human frontal cortex—Development and deficits in schizophrenia. *J. Chem. Neuroanat.* **22**, 95–100 (2001).
19. D. W. Volk, J. R. Edelson, D. A. Lewis, Altered expression of developmental regulators of parvalbumin and somatostatin neurons in the prefrontal cortex in schizophrenia. *Schizophr. Res.* **177**, 3–9 (2016).
20. H. M. Morris, T. Hashimoto, D. A. Lewis, Alterations in somatostatin mRNA expression in the dorsolateral prefrontal cortex of subjects with schizophrenia or schizoaffective disorder. *Cereb. Cortex* **18**, 1575–1587 (2008).
21. D. J. Holt, M. M. Herman, T. M. Hyde, J. E. Kleinman, C. M. Sinton, D. C. German, L. B. Hersh, A. M. Graybiel, C. B. Saper, Evidence for a deficit in cholinergic interneurons in the striatum in schizophrenia. *Neuroscience* **94**, 21–31 (1999).
22. I. Adorjan, B. Sun, V. Feher, T. Tyler, D. Veres, S. A. Chance, F. G. Szele, Evidence for decreased density of calretinin-immunopositive neurons in the caudate nucleus in patients with schizophrenia. *Front. Neuroanat.* **14**, 581685 (2020).
23. H. Pantazopoulos, J. T. Wiseman, M. Markota, L. Ehrenfeld, S. Berretta, Decreased numbers of somatostatin-expressing neurons in the amygdala of subjects with bipolar disorder or schizophrenia: Relationship to circadian rhythms. *Biol. Psychiatry* **81**, 536–547 (2017).
24. M. Fromer, P. Roussos, S. K. Sieberts, J. S. Johnson, D. H. Kavanagh, T. M. Perumal, D. M. Ruderfer, E. C. Oh, A. Topol, H. R. Shah, L. L. Klei, R. Kramer, D. Pinto, Z. H. Gumus, A. E. Cicek, K. K. Dang, A. Browne, C. Lu, L. Xie, B. Readhead, E. A. Stahl, J. Xiao, M. Parvizi, T. Hamamsy, J. F. Fullard, Y. C. Wang, M. C. Mahajan, J. M. Derry, J. T. Dudley, S. E. Hemby, B. A. Logsdon, K. Talbot, T. Raj, D. A. Bennett, P. L. De Jager, J. Zhu, B. Zhang, P. F. Sullivan, A. Chess, S. M. Purcell, L. A. Shinobu, L. M. Mangravite, H. Toyoshiba, R. E. Gur, C. G. Hahn, D. A. Lewis, V. Haroutunian, M. A. Peters, B. K. Lipska, J. D. Buxbaum, E. E. Schadt, K. Hirai, K. Roeder, K. J. Brennand, N. Katsanis, E. Domenici, B. Devlin, P. Sklar, Gene expression elucidates functional impact of polygenic risk for schizophrenia. *Nat. Neurosci.* **19**, 1442–1453 (2016).
25. E. F. W. Bowen, J. L. Burgess, R. Granger, J. E. Kleinman, C. H. Rhodes, DLPFC transcriptome defines two molecular subtypes of schizophrenia. *Transl. Psychiatry* **9**, 147 (2019).
26. S. G. Fillman, N. Cloonan, V. S. Catts, L. C. Miller, J. Wong, T. McCrossin, M. Cairns, C. S. Weickert, Increased inflammatory markers identified in the dorsolateral prefrontal cortex of individuals with schizophrenia. *Mol. Psychiatry* **18**, 206–214 (2013).
27. J. N. Pierri, C. L. E. Volk, S. Auh, A. Sampson, D. A. Lewis, Decreased somal size of deep layer 3 pyramidal neurons in the prefrontal cortex of subjects with schizophrenia. *Arch. Gen. Psychiatry* **58**, 466–473 (2001).
28. A. J. Holmes, A. MacDonald III, C. S. Carter, D. M. Barch, V. A. Stenger, J. D. Cohen, Prefrontal functioning during context processing in schizophrenia and major depression: An event-related fMRI study. *Schizophr. Res.* **76**, 199–206 (2005).
29. A. W. MacDonald III, C. S. Carter, J. G. Kerns, S. Ursu, D. M. Barch, A. J. Holmes, V. A. Stenger, J. D. Cohen, Specificity of prefrontal dysfunction and context processing deficits to schizophrenia in never-medicated patients with first-episode psychosis. *Am. J. Psychiatry* **162**, 475–484 (2005).
30. U. Pfisterer, V. Petukhov, S. Demharter, J. Meichsner, J. J. Thompson, M. Y. Batiuk, A. A. Martinez, N. A. Vasistha, A. Thakur, J. Mikkelsen, I. Adorjan, L. H. Pinborg, T. H. Pers, J. von Engelhardt, P. V. Kharchenko, K. Khodosevich, Identification of epilepsy-associated neuronal subtypes and gene expression underlying epileptogenesis. *Nat. Commun.* **11**, 5038 (2020).
31. N. Barkas, V. Petukhov, D. Nikolaeva, Y. Lozinsky, S. Demharter, K. Khodosevich, P. V. Kharchenko, Joint analysis of heterogeneous single-cell RNA-seq dataset collections. *Nat. Methods* **16**, 695–698 (2019).
32. R. D. Hodge, T. E. Bakken, J. A. Miller, K. A. Smith, E. R. Barkan, L. T. Graybuck, J. L. Close, B. Long, N. Johansen, O. Penn, Z. Yao, J. Eggermont, T. Höllt, B. P. Levi, S. I. Shehata, B. Aevermann, A. Beller, D. Bertagnolli, K. Brouner, T. Casper, C. Cobbs, R. Dalley, N. Dee, S. L. Ding, R. G. Ellenbogen, O. Fong, E. Garren, J. Goldy, R. P. Gwinn, D. Hirschstein, C. D. Keene, M. Keshk, A. L. Ko, K. Lathia, A. Mahfouz, Z. Maltzer, M. McGraw, T. N. Nguyen, J. Nyhus, J. G. Ojemann, A. Oldre, S. Parry, S. Reynolds, C. Rimorin, N. V. Shapovalova, S. Somasundaram, A. Szafer, E. R. Thomsen, M. Tieu, G. Quon, R. H. Scheuermann, R. Yuste, S. M. Sunkin, B. Lelieveldt, D. Feng, L. Ng, A. Bernard, M. Hawrylycz, J. W. Phillips, B. Tasic, H. Zeng, A. R. Jones, C. Koch, E. S. Lein, Conserved cell types with divergent features in human versus mouse cortex. *Nature* **573**, 61–68 (2019).
33. Allen Institute Cell Types Database: RNA-Seq Data; Multiple Cortical Areas - SMART-SEQ (2019). *Database* (2019).
34. V. Pawlowsky-Glahn, A. Buccianti, *Compositional Data Analysis* (John Wiley & Sons Ltd., 2011).
35. Y. Kfoury, N. Baryawno, N. Severe, S. Mei, K. Gustafsson, T. Hirz, T. Brouse, E. W. Scadden, A. A. Igolkina, K. Kokkaliaris, B. D. Choi, N. Barkas, M. A. Randolph, J. H. Shin, P. J. Saylor, D. T. Scadden, D. B. Sykes, P. V. Kharchenko, Human prostate cancer bone metastases have an actionable immunosuppressive microenvironment. *Cancer Cell* **39**, 1464–1478.e8 (2021).
36. G. E. Hoffman, J. Bendl, G. Voloudakis, K. S. Montgomery, L. Sloofman, Y. C. Wang, H. R. Shah, M. E. Hauberg, J. S. Johnson, K. Girdhar, L. Song, J. F. Fullard, R. Kramer, C. G. Hahn, R. Gur, S. Marenco, B. K. Lipska, D. A. Lewis, V. Haroutunian, S. Hemby, P. Sullivan, S. Akbarian, A. Chess, J. D. Buxbaum, G. E. Crawford, E. Domenici, B. Devlin, S. K. Sieberts, M. A. Peters, P. Roussos, CommonMind Consortium provides transcriptomic and epigenomic data for Schizophrenia and Bipolar Disorder. *Sci. Data* **6**, 180 (2019).
37. C. C. Bell, DSM-IV: Diagnostic and statistical manual of mental disorders. *J. Am. Med. Assoc.* **272**, 828 (1994).
38. J. Defelipe, The evolution of the brain, the human nature of cortical circuits, and intellectual creativity. *Front. Neuroanat.* **5**, 29 (2011).
39. H. Mohan, M. B. Verhoog, K. K. Doreswamy, G. Eyal, R. Aardse, B. N. Lodder, N. A. Goriounova, B. Asamoah, A. B. B. C. B. Brakspear, C. Groot, S. Van Der Sluis, G. Testa-Silva, J. Obermayer, Z. S. R. M. Boudewijns, R. T. Narayanan, J. C. Baayen, I. Segev, H. D. Mansvelder, C. P. J. De Kock, Dendritic and axonal architecture of individual pyramidal neurons across layers of adult human neocortex. *Cereb. Cortex* **25**, 4839–4853 (2015).
40. J. Berg, S. A. Sorensen, J. T. Ting, J. A. Miller, T. Chartrand, A. Buchin, T. E. Bakken, A. Budzillo, N. Dee, S. L. Ding, N. W. Gouwens, R. D. Hodge, B. Kalmbach, C. Lee, B. R. Lee, L. Alfiler, K. Baker, E. Barkan, A. Beller, K. Berry, D. Bertagnolli, K. Bickley, J. Bomben, T. Braun, K. Brouner, T. Casper, P. Chong, K. Crichton, R. Dalley, R. de Frates, T. Desta, S. D. Lee, F. D'Orazi, N. Dotson, T. Egdorf, R. Enstrom, C. Farrell, D. Feng, O. Fong, S. Furdan, A. A. Galakhova, C. Gamlin, A. Gary, A. Glandon, J. Goldy, M. Gorham, N. A. Goriounova, S. Gratiy, L. Graybuck, H. Gu, K. Hadley, N. Hansen, T. S. Heistek,

A. M. Henry, D. B. Heyer, D. J. Hill, C. Hill, M. Hupp, T. Jarsky, S. Kebede, L. Keene, L. Kim, M. H. Kim, M. Kroll, C. Latimer, B. P. Levi, K. E. Link, M. Mallory, R. Mann, D. Marshall, M. Maxwell, M. McGraw, D. McMillen, E. Melief, E. J. Mertens, L. Mezei, N. Mihut, S. Mok, G. Molnar, A. Mukora, L. Ng, K. Ngo, P. R. Nicovich, J. Nyhus, G. Olah, A. Oldre, V. Omstead, A. Ozsvar, D. Park, H. Peng, T. Pham, C. A. Pom, L. Potekhina, R. Rajanbabu, S. Ransford, D. Reid, C. Rimorin, A. Ruiz, D. Sandman, J. Sulc, S. M. Sunkin, A. Szafer, V. Szemenyei, E. R. Thomsen, M. Tieu, A. Torkelson, J. Trinh, H. Tung, W. Wakeman, F. Waleboer, K. Ward, R. Wilbers, G. Williams, Z. Yao, J. G. Yoon, C. Anastassiou, A. Arkhipov, P. Barzo, A. Bernard, C. Cobbs, P. C. de Witt Hamer, R. G. Ellenbogen, L. Esposito, M. Ferreira, R. P. Gwinn, M. J. Hawrylycz, P. R. Hof, S. Idema, A. R. Jones, C. D. Keene, A. L. Ko, G. J. Murphy, L. Ng, J. G. Ojemann, A. P. Patel, J. W. Phillips, D. L. Silbergeld, K. Smith, B. Tasic, R. Yuste, I. Segev, C. P. J. de Kock, H. D. Mansvelder, G. Tamas, H. Zeng, C. Koch, E. S. Lein, Human neocortical expansion involves glutamatergic neuron diversification. *Nature* **598**, 151–158 (2021).

41. T. E. Bakken, N. L. Jorstad, Q. Hu, B. B. Lake, W. Tian, B. E. Kalmbach, M. Crow, R. D. Hodge, F. M. Krienen, S. A. Sorensen, J. Eggermont, Z. Yao, B. D. Aevermann, A. I. Aldridge, A. Bartlett, D. Bertagnolli, T. Casper, R. G. Castanon, K. Crichton, T. L. Daigle, R. Dalley, N. Dee, N. Dembrow, D. Diep, S. L. Ding, W. Dong, R. Fang, S. Fischer, M. Goldman, J. Goldy, L. T. Graybuck, B. R. Herb, X. Hou, J. Kancherla, M. Kroll, K. Lathia, B. van Lew, Y. E. Li, C. S. Liu, H. Liu, J. D. Lucero, A. Mahurkar, D. McMillen, J. A. Miller, M. Moussa, J. R. Nery, P. R. Nicovich, S. Y. Niu, J. Orvis, J. K. Osteen, S. Owen, C. R. Palmer, T. Pham, N. Plongthongkum, O. Poirion, N. M. Reed, C. Rimorin, A. Rivkin, W. J. Romanow, A. E. Sedeño-Cortés, K. Siletti, S. Somasundaram, J. Sulc, M. Tieu, A. Torkelson, H. Tung, X. Wang, F. Xie, A. M. Yanny, R. Zhang, S. A. Ament, M. M. Behrens, H. C. Bravo, J. Chun, A. Dobin, J. Gillis, R. Hertzano, P. R. Hof, T. Höllt, G. D. Horwitz, C. D. Keene, P. V. Kharchenko, A. L. Ko, B. P. Lelieveldt, C. Luo, E. A. Mukamel, A. Pinto-Duarte, S. Preissl, A. Regev, B. Ren, R. H. Scheuermann, K. Smith, W. J. Spain, O. R. White, C. Koch, M. Hawrylycz, B. Tasic, E. Z. Macosko, S. A. McCarroll, J. T. Ting, H. Zeng, K. Zhang, G. Feng, J. R. Ecker, S. Linnarsson, E. S. Lein, Comparative cellular analysis of motor cortex in human, marmoset and mouse. *Nature* **598**, 111–119 (2021).
42. A. Hladnik, D. Džaja, S. Darmopil, N. Jovanov-Milošević, Z. Petanjek, Spatio-temporal extension in site of origin for cortical calretinin neurons in primates. *Front. Neuroanat.* **8**, 50 (2014).
43. M. L. Sinkus, S. Graw, R. Freedman, R. G. Ross, H. A. Lester, S. Leonard, The human CHRNA7 and CHRFAM7A genes: A review of the genetics, regulation, and function. *Neuropharmacology* **96**, 274–288 (2015).
44. K. A. Perzel Mandell, N. J. Eagles, A. Deep-Soboslay, R. Tao, S. Han, R. Wilton, A. S. Szalay, T. M. Hyde, J. E. Kleinman, A. E. Jaffe, D. R. Weinberger, Molecular phenotypes associated with antipsychotic drugs in the human caudate nucleus. *Mol. Psychiatry* **27**, 2061–2067 (2022).
45. T. Hashimoto, D. Arion, T. Unger, J. G. Maldonado-Avilés, H. M. Morris, D. W. Volk, K. Mirnics, D. A. Lewis, Alterations in GABA-related transcriptome in the dorsolateral prefrontal cortex of subjects with schizophrenia. *Mol. Psychiatry* **13**, 147–161 (2008).
46. C. Montag, E.-M. Brockmann, A. Lehmann, D. J. Müller, D. Rujescu, J. Gallinat, Association between oxytocin receptor gene polymorphisms and self-rated 'empathic concern' in schizophrenia. *PLOS ONE* **7**, e51882 (2012).
47. C. H. Holland, J. Tanevski, J. Perales-Patón, J. Gleixner, M. P. Kumar, E. Mereu, B. A. Joughin, O. Stegle, D. A. Lauffenburger, H. Heyn, B. Szalai, J. Saez-Rodriguez, Robustness and applicability of transcription factor and pathway analysis tools on single-cell RNA-seq data. *Genome Biol.* **21**, 36 (2020).
48. M. J. Alvarez, Y. Shen, F. M. Giorgi, A. Lachmann, B. B. Ding, B. Hilda Ye, A. Califano, Functional characterization of somatic mutations in cancer using network-based inference of protein activity. *Nat. Genet.* **48**, 838–847 (2016).
49. K. A. Aberg, J. L. McClay, S. Nerella, S. Clark, G. Kumar, W. Chen, A. N. Khachane, L. Xie, A. Hudson, G. Gao, A. Harada, C. M. Hultman, P. F. Sullivan, P. K. E. Magnusson, E. J. C. G. Van Den Oord, Methylome-wide association study of schizophrenia: Identifying blood biomarker signatures of environmental insults. *JAMA Psychiatry* **71**, 255–264 (2014).
50. M. Lam, W. D. Hill, J. W. Trampush, J. Yu, E. Knowles, G. Davies, E. Stahl, L. Huckins, D. C. Liewald, S. Djurovic, I. Melle, K. Sundet, A. Christoforou, I. Reinvang, P. DeRosse, A. J. Lundervold, V. M. Steen, T. Espeseth, K. Räikkönen, E. Widen, A. Palotie, J. G. Eriksson, I. Giegling, B. Konte, A. M. Hartmann, P. Roussos, S. Giakoumaki, K. E. Burdick, A. Payton, W. Ollier, O. Chiba-Falek, D. K. Attix, A. C. Need, E. T. Cirulli, A. N. Voineskos, N. C. Stefanis, D. Avramopoulos, A. Hatzimanolis, D. E. Arking, N. Smyrnis, R. M. Bilder, N. A. Freimer, T. D. Cannon, E. London, R. A. Poldrack, F. W. Sabb, E. Congdon, E. D. Conley, M. A. Scult, D. Dickinson, R. E. Straub, G. Donohoe, D. Morris, A. Corvin, M. Gill, A. R. Hariri, D. R. Weinberger, N. Pendleton, P. Bitsios, D. Rujescu, J. Lahti, S. Le Hellard, M. C. Keller, O. A. Andreassen, I. J. Deary, D. C. Glahn, A. K. Malhotra, T. Lencz, Pleiotropic meta-analysis of cognition, education, and schizophrenia differentiates roles of early neurodevelopmental and adult synaptic pathways. *Am. J. Hum. Genet.* **105**, 334–350 (2019).
51. F. S. Goes, J. Mcgrath, D. Avramopoulos, P. Wolyniec, M. Pirooznia, I. Ruczinski, G. Nestadt, E. E. Kenny, V. Vacic, I. Peters, T. Lencz, A. Darvasi, J. G. Mulle, S. T. Warren, A. E. Pulver, Genome-wide association study of schizophrenia in Ashkenazi Jews. *Am. J. Med. Genet. B Neuropsychiatr. Genet.* **168**, 649–659 (2015).
52. K. A. Aberg, Y. Liu, J. Bukszár, J. L. McClay, A. N. Khachane, O. A. Andreassen, D. Blackwood, A. Corvin, S. Djurovic, H. Gurling, R. Ophoff, C. N. Pato, M. T. Pato, B. Riley, T. Webb, K. Kendler, M. O'Donovan, N. Craddock, G. Kirov, M. Owen, D. Rujescu, D. S. Clair, T. Werge, C. M. Hultman, L. E. Delisi, P. Sullivan, E. J. Van Den Oord, A comprehensive family-based replication study of schizophrenia genes. *JAMA Psychiatry* **70**, 573–581 (2013).
53. B. Ruzicka, S. Mohammadi, J. Davila-Velderrain, S. Subburaju, D. Reed, M. Hourihan, M. Kellis, Single-cell dissection of schizophrenia reveals neurodevelopmental-synaptic axis and transcriptional resilience. *medRxiv* 10.1101/2020.11.06.20225342 , (2020).
54. L. M. Huckins, A. Dobbyn, D. M. Ruderfer, G. Hoffman, W. Wang, A. F. Pardiñas, V. M. Rajagopal, T. D. Als, H. T. Nguyen, K. Girdhar, J. Boocock, P. Roussos, M. Fromer, R. Kramer, E. Domenici, E. R. Gamazon, S. Purcell; CommonMind Consortium; Schizophrenia Working Group of the Psychiatric Genomics Consortium; iPSYCH-GEMS Schizophrenia Working Group, D. Demontis, A. D. Børglum, J. T. R. Walters, M. C. O'Donovan, P. Sullivan, M. J. Owen, B. Devlin, S. K. Sieberts, N. J. Cox, H. K. Im, P. Sklar, E. A. Stahl, Gene expression imputation across multiple brain regions provides insights into schizophrenia risk. *Nat. Genet.* **51**, 659–674 (2019).
55. J. R. Teixeira, R. A. Szeto, V. M. A. Carvalho, A. R. Muotri, F. Papes, Transcription factor 4 and its association with psychiatric disorders. *Transl. Psychiatry* **11**, 19 (2021).
56. S. Le Hellard, T. W. Mühleisen, S. Djurovic, J. Fernø, Z. Ouriaghi, M. Mattheisen, C. Vasilescu, M. B. Raeder, T. Hansen, J. Strohmaier, A. Georgi, F. F. Brockschmidt, I. Melle, I. Nenadic, H. Sauer, M. Rietschel, M. M. Nöthen, T. Werge, O. A. Andreassen, S. Cichon, V. M. Steen, Polymorphisms in SREBF1 and SREBF2, two antipsychotic-activated transcription factors controlling cellular lipogenesis, are associated with schizophrenia in German and Scandinavian samples. *Mol. Psychiatry* **15**, 463–472 (2010).
57. D. J. Araujo, K. Toriumi, C. O. Escamilla, A. Kulkarni, A. G. Anderson, M. Harper, N. Usui, J. Ellegood, J. P. Lerch, S. G. Birnbaum, H. O. Tucker, C. M. Powell, G. Konopka, Foxp1 in forebrain pyramidal neurons controls gene expression required for spatial learning and synaptic plasticity. *J. Neurosci.* **37**, 10917–10931 (2017).
58. S. V. Hegarty, A. M. Sullivan, G. W. O'Keeffe, Zeb2: A multifunctional regulator of nervous system development. *Prog. Neurobiol.* **132**, 81–95 (2015).
59. A. Barešić, A. J. Nash, T. Dahoun, O. Howes, B. Lenhard, Understanding the genetics of neuropsychiatric disorders: The potential role of genomic regulatory blocks. *Mol. Psychiatry* **25**, 6–18 (2020).
60. J. Piñero, Á. Bravo, N. Queralt-Rosinach, A. Gutiérrez-Sacristán, J. Deu-Pons, E. Centeno, J. García-García, F. Sanz, L. I. Furlong, DisGeNET: A comprehensive platform integrating information on human disease-associated genes and variants. *Nucleic Acids Res.* **45**, D833–D839 (2017).
61. A. F. Pardiñas, P. Holmans, A. J. Pocklington, V. Escott-Price, S. Ripke, N. Carrera, S. E. Legge, S. Bishop, D. Cameron, M. L. Hamshere, J. Han, L. Hubbard, A. Lynham, K. Mantripragada, E. Rees, J. H. MacCabe, S. A. McCarroll, B. T. Baune, G. Breen, E. M. Byrne, U. Dannlowski, T. C. Eley, C. Hayward, N. G. Martin, A. M. McIntosh, R. Plomin, D. J. Porteous, N. R. Wray, A. Caballero, D. H. Geschwind, L. M. Huckins, D. M. Ruderfer, E. Santiago, P. Sklar, E. A. Stahl, H. Won, E. Agerbo, T. D. Als, O. A. Andreassen, M. Bækvad-Hansen, P. B. Mortensen, C. B. Pedersen, A. D. Børglum, J. Bybjerg-Grauholm, S. Djurovic, N. Durmishi, M. G. Pedersen, V. Golimbet, J. Grove, D. M. Hougaard, M. Mattheisen, E. Molden, O. Mors, M. Nordentoft, M. Pejovic-Milovancevic, E. Sigurdsson, T. Silagadze, C. S. Hansen, K. Stefansson, H. Stefansson, S. Steinberg, S. Tosato, T. Werge; GERAD1 Consortium; CRESTAR Consortium, D. A. Collier, G. Kirov, M. J. Owen, M. C. O'Donovan, J. T. R. Walters, Common schizophrenia alleles are enriched in mutation-intolerant genes and in regions under strong background selection. *Nat. Genet.* **50**, 381–389 (2018).
62. F. M. Krienen, M. Goldman, Q. Zhang, R. C. H. del Rosario, M. Florio, R. Machold, A. Saunders, K. Levandowski, H. Zaniewski, B. Schuman, C. Wu, A. Lutservitz, C. D. Mullally, N. Reed, E. Bien, L. Bortolin, M. Fernandez-Otero, J. D. Lin, A. Wysoker, J. Nemesh, D. Kulp, M. Burns, V. Tkachev, R. Smith, C. A. Walsh, J. Dimidschstein, B. Rudy, L. S. Kean, S. Berretta, G. Fishell, G. Feng, S. A. McCarroll, Innovations present in the primate interneuron repertoire. *Nature* **586**, 262–269 (2020).
63. Z. Petanjek, D. Sedmak, D. Džaja, A. Hladnik, M. R. Rašin, N. Jovanov-Milosevic, The Protracted maturation of associative layer IIIC pyramidal neurons in the human prefrontal cortex during childhood: A major role in cognitive development and selective alteration in autism. *Front. Psychiatry* **10**, 122 (2019).
64. N. Zecevic, P. Rakic, Development of layer I neurons in the primate cerebral cortex. *J. Neurosci.* **21**, 5607–5619 (2001).
65. M. Li, G. Santpere, Y. I. Kawasawa, O. V. Evgrafov, F. O. Gulden, S. Pochareddy, S. M. Sunkin, Z. Li, Y. Shin, Y. Zhu, A. M. M. Sousa, D. M. Werling, R. R. Kitchen, H. J. Kang, M. Pletikos, J. Choi, S. Muchnik, X. Xu, D. Wang, B. Lorente-Galdos, S. Liu, P. Giusti-Rodríguez, H. Won, C. A. de Leeuw, A. F. Pardiñas; BrainSpan Consortium; PsychENCODE Consortium; PsychENCODE Developmental Subgroup, M. Hu, F. Jin, Y. Li, M. J. Owen, M. C. O'Donovan,

J. T. R. Walters, D. Posthuma, M. A. Reimers, P. Levitt, D. R. Weinberger, T. M. Hyde, J. E. Kleinman, D. H. Geschwind, M. J. Hawrylycz, M. W. State, S. J. Sanders, P. F. Sullivan, M. B. Gerstein, E. S. Lein, J. A. Knowles, N. Sestan, Integrative functional genomic analysis of human brain development and neuropsychiatric risks. *Science* **362**, eaat7615 (2018).
66. J. C. Silbereis, S. Pochareddy, Y. Zhu, M. F. Li, N. Sestan, The cellular and molecular landscapes of the developing human central nervous system. *Neuron* **89**, 248–268 (2016).
67. Z. Petanjek, M. Judaš, G. Šimić, M. R. Rašin, H. B. M. Uylings, P. Rakic, I. Kostović, Extraordinary neoteny of synaptic spines in the human prefrontal cortex. *Proc. Natl. Acad. Sci. U.S.A.* **108**, 13281–13286 (2011).
68. D. Velmeshev, L. Schirmer, D. Jung, M. Haeussler, Y. Perez, S. Mayer, A. Bhaduri, N. Goyal, D. H. Rowitch, A. R. Kriegstein, Single-cell genomics identifies cell type–specific molecular changes in autism. *Science* **364**, 685–689 (2019).
69. D. Wang, S. Liu, J. Warrell, H. Won, X. Shi, F. C. P. Navarro, D. Clarke, M. Gu, P. Emani, Y. T. Yang, M. Xu, M. J. Gandal, S. Lou, J. Zhang, J. J. Park, C. Yan, S. K. Rhie, K. Manakongtreecheep, H. Zhou, A. Nathan, M. Peters, E. Mattei, D. Fitzgerald, T. Brunetti, J. Moore, Y. Jiang, K. Girdhar, G. E. Hoffman, S. Kalayci, Z. H. Gümüş, G. E. Crawford; PsychENCODE Consortium, P. Roussos, S. Akbarian, A. E. Jaffe, K. P. White, Z. Weng, N. Sestan, D. H. Geschwind, J. A. Knowles, M. B. Gerstein, Comprehensive functional genomic resource and integrative model for the human brain. *Science* **362**, eaat8464 (2018).
70. O. Yizhar, O. Klavir, Reciprocal amygdala–prefrontal interactions in learning. *Curr. Opin. Neurobiol.* **52**, 149–155 (2018).
71. D. Heyer, R. Wilbers, A. Galakhova, E. Hartsema, S. Braak, S. Hunt, M. Verhoog, M. Muijtjens, E. Mertens, S. Idema, J. Baayen, P. de Witt Hamer, M. Klein, M. McGraw, E. S. Lein, C. P. J. de Kock, H. D. Mansvelder, N. Goriounova, Expansion of cortical layers 2 and 3 in human left temporal cortex associates with verbal intelligence. bioRxiv 2021.02.07.430103 [**Preprint**]. 7 February 2021. https://doi.org/10.1101/2021.02.07.430103.
72. O. A. Bjorkquist, E. K. Olsen, B. D. Nelson, E. S. Herbener, Altered amygdala-prefrontal connectivity during emotion perception in schizophrenia. *Schizophr. Res.* **175**, 35–41 (2016).
73. P. V. Viher, L. Docx, W. Van Hecke, P. M. Parizel, B. Sabbe, A. Federspiel, S. Walther, M. Morrens, Aberrant fronto-striatal connectivity and fine motor function in schizophrenia. *Psychiatry Res. Neuroimaging* **288**, 44–50 (2019).
74. V. Molina, A. Lubeiro, J. Blanco, J. A. Blanco, M. Rodríguez, A. Rodríguez-Campos, R. de Luis-García, Parkinsonism is associated to fronto-caudate disconnectivity and cognition in schizophrenia. *Psychiatry Res. Neuroimaging.* **277**, 1–6 (2018).
75. V. Petukhov, A. Igolkina, R. Rydbirk, S. Mei, L. Christoffersen, K. Khodosevich, P. V. Kharchenko, Case-control analysis of single-cell RNA-seq studies. bioRxiv 2022.03.15.484475 [**Preprint**]. 18 March 2022. https://doi.org/10.1101/2022.03.15.484475.
76. E. M. Schoof, B. Furtwängler, N. Üresin, N. Rapin, S. Savickas, C. Gentil, E. Lechman, U. auf dem Keller, J. E. Dick, B. T. Porse, Quantitative single-cell proteomics as a tool to characterize cellular hierarchies. *Nat. Commun.* **12**, 3341 (2021).
77. X. Wang, J. Park, K. Susztak, N. R. Zhang, M. Li, Bulk tissue cell type deconvolution with multi-subject single-cell expression reference. *Nat. Commun.* **10**, 380 (2019).
78. M. I. Love, W. Huber, S. Anders, Moderated estimation of fold change and dispersion for RNA-seq data with DESeq2. *Genome Biol.* **15**, 550 (2014).
79. J. W. Squair, M. Gautier, C. Kathe, M. A. Anderson, N. D. James, T. H. Hutson, R. Hudelle, T. Qaiser, K. J. E. Matson, Q. Barraud, A. J. Levine, G. La Manno, M. A. Skinnider, G. Courtine, Confronting false discoveries in single-cell differential expression. *Nat. Commun.* **12**, 5692 (2021).
80. G. Yu, L.-G. Wang, Y. Han, Q.-Y. He, clusterProfiler: An R package for comparing biological themes among gene clusters. *OMICS* **16**, 284–287 (2012).
81. P. N. Timshel, J. J. Thompson, T. H. Pers, Genetic mapping of etiologic brain cell types for obesity. *eLife* **9**, e55851 (2020).
82. G. Pertea, M. Pertea, GFF utilities: GffRead and GffCompare. *F1000Res.* **9**, 304 (2020).
83. J. Schindelin, I. Arganda-Carreras, E. Frise, V. Kaynig, M. Longair, T. Pietzsch, S. Preibisch, C. Rueden, S. Saalfeld, B. Schmid, J. Y. Tinevez, D. J. White, V. Hartenstein, K. Eliceiri, P. Tomancak, A. Cardona, Fiji: An open-source platform for biological-image analysis. *Nat. Methods* **9**, 676–682 (2012).
84. BRAIN Initiative Cell Census Network (BICCN), A multimodal cell census and atlas of the mammalian primary motor cortex. *Nature* **598**, 86–102 (2021).
85. T. Stuart, A. Butler, P. Hoffman, C. Hafemeister, E. Papalexi, W. M. Mauck III, Y. Hao, M. Stoeckius, P. Smibert, R. Satija, Comprehensive integration of single-cell data. *Cell* **177**, 1888–1902.e21 (2019).
86. I. Adorjan, B. Ahmed, V. Feher, M. Torso, K. Krug, M. Esiri, S. A. Chance, F. G. Szele, Calretinin interneuron density in the caudate nucleus is lower in autism spectrum disorder. *Brain* **140**, 2028–2040 (2017).
87. M. Petrides, D. N. Pandya, Dorsolateral prefrontal cortex: Comparative cytoarchitectonic analysis in the human and the macaque brain and corticocortical connection patterns. *Eur. J. Neurosci.* **11**, 1011–1036 (1999).
88. B. R. Rocco, R. A. Sweet, D. A. Lewis, K. N. Fish, GABA-synthesizing enzymes in calbindin and calretinin neurons in monkey prefrontal cortex. *Cereb. Cortex* **26**, 2191–2204 (2016).
89. F. Billwiller, L. Castillo, H. Elseedy, A. I. Ivanov, J. Scapula, A. Ghestem, J. Carponcy, P. A. Libourel, H. Bras, N. E. S. Abdelmeguid, E. Krook-Magnuson, I. Soltesz, C. Bernard, P. H. Luppi, M. Esclapez, GABA–glutamate supramammillary neurons control theta and gamma oscillations in the dentate gyrus during paradoxical (REM) sleep. *Brain Struct. Funct.* **1**, 2643–2668 (2020).
90. J. Pinheiro, D. Bates, S. DebRoy, D. Sarkar, S. Heisterkamp, B. Van Willigen, Linear and nonlinear mixed effects models contact: Package 'nlme' (2020);https://bugs.r-project.org.

Acknowledgments: We are grateful to I. Korshunova, M. Bako, J. Kerti, Z. E. Toth, B. Popovic, and M. Horvat for technical assistance. We thank C. Sloan, H. Brooks, M. Palkovits, E. Renner, M. Kooreman, and D. Lennard (Human Tissue Brain Bank at Semmelweis University, Oxford Brain Bank, the Netherlands Brain Bank, and Newcastle Brain Bank) for assistance in procuring human brain tissue. We thank Z. Lang and D. Veres for comments on statistical analysis of IHC and in situ hybridization data. We are also grateful to A. Andersson for comments on spatial transcriptomics analysis and E. Ocheredko for initial help with data analysis. We thank BRIC's single cell (I. Korshunova), flow cytometry (A. Fossum and R. Somasundaram), imaging (Y. Antoku), and sequencing (F. Rodriguez Gonzalez) core facilities as well as CBMR sequencing core facility (K. Egerod) for assistance during this work. We are also grateful to Technical University of Denmark for providing computational infrastructure at Danish National Supercomputer for Life Sciences (Computerome). **Funding:** The work was supported by Novo Nordisk Hallas-Møller Investigator grants (NNF16OC0019920 and NNF21OC0067146), Lundbeckfonden–NIH Brain Initiative grant (2017-2241), Lundbeckfonden Ascending Investigator grant (2020-1025), and Independent Research Fund Denmark (8020-00083B) to K.K. The study was funded by the Institutional Excellence in Higher Education Grant (FIKP), STIA_18, TeT 2019-2021, Thematic Excellence Programme 2020-2021, and Departmental Start-up Grants (Semmelweis University) to I.A. T.T. was supported by the ÚNKP-19-2 New National Excellence Programme of the Ministry for Innovation and Technology (Hungary) and STIA-2020 Grant (Semmelweis University). The work of D.S., N.H., and Z.P. was supported by Croatian Science Foundation grant no. 5943 (Microcircuitry of higher cognitive functions, principal investigator: Z.P.) and the European Union through the European Regional Development Fund, Operational Programme Competitiveness and Cohesion, grant agreement no. KK.01.1.1.01.0007, CoRE—Neuro. R.D. was supported by a Ministry of Science and High Education of the Russian Federation (agreement no. 075-15-2020-784). **Author contributions:** K.K. and M.Y.B. designed snRNA-seq and Visium experiments. M.Y.B. performed nucleus preparation and FACS experiments and performed snRNA-seq library preparation and Visium library preparation. M.Y.B. developed modified protocol for nucleus isolation. I.A. designed histological experiments. T.T., E.F., V.F., and L.R. performed histological experiments. T.T., I.A., and M.Y.B. analyzed histological and in situ hybridization data. N.H., D.S., and Z.P. designed and executed in situ hybridization experiments. P.V.K. developed novel algorithms for snRNA-seq data analysis. P.V.K., K.D., M.Y.B., R.R., V.P., S.M., Q.H., A.I., and R.D. analyzed snRNA-seq and bulk RNA-seq data. P.V.K., K.D., V.P., and M.Y.B. analyzed spatial transcriptomics data. M.Y.B. and D.G.-G. processed tissue for spatial transcriptomics. U.P. performed initial snRNA-seq trial experiments. Z.P. supervised in situ hybridization experiments. I.A. supervised histological experiments. P.V.K. and K.K. supervised data analysis of snRNA-seq and spatial transcriptomics data. K.K., P.V.K., and I.A. conceived and directed the project. K.K., P.V.K., and I.A. wrote the manuscript with significant input from M.Y.B., T.T., and K.D. M.Y.B. and T.T. are equal first authors, and I.A., P.V.K., and K.K. are equal last authors of the paper. All authors read and gave input during manuscript writing. All authors approved submission. **Competing interests:** P.V.K. serves on the Scientific Advisory Board to Celsius Therapeutics Inc. and Biomage Inc. The other authors declare that they have no competing interests. **Data and materials availability:** Code to reproduce the analysis is available on Github (https://github.com/khodosevichlab/Schizophrenia20) and archived at Zenodo (https://doi.org/10.5281/zenodo.6583332). Raw snRNA-seq count matrices, snRNA-seq Conos object, Visium raw count matrices, Visium spaceranger count pipeline output files, manually assigned cortical layers for Visium samples, and histological images of Visium samples are available at https://doi.org/10.5281/zenodo.6921620. Supplementary Dataset Tables 1 to 4 are available at https://doi.org/10.5281/zenodo.6921620. The raw snRNA-seq data are available at EGA, EGAS00001006495 (https://ega-archive.org/studies/EGAS00001006495). Access to scanned and analyzed microscopy images can be provided upon request from I.A. (neuropsych.lab.se@gmail.com) due to their large file size.

Submitted 22 December 2021
Accepted 24 August 2022
Published 12 October 2022
10.1126/sciadv.abn8367